

Contribution of a deformable striking-ship structure to the structural crashworthiness of ship-ship collisions

Yeong Gook Ko^a, Sang Jin Kim^b, Jeom Kee Paik^{a,b,c,*}

^a Department of Naval Architecture and Ocean Engineering, Pusan National University, Busan 46241, Republic of Korea

^b The Korea Ship and Offshore Research Institute (The Lloyd's Register Foundation Research Centre of Excellence), Pusan National University, Busan 46241, Republic of Korea

^c Department of Mechanical Engineering, University College London, London, WC1E 7JE, UK

Abstract

Ship-ship collision is one of the most frequent types of accidents in shipping industry. The risks of massive financial losses and marine pollution have been increasing due to ship-ship collisions where large oil tankers or liquefied natural gas (LNG)-fueled ships can be involved in the accidents. Various types of methods are available for the purpose of safety studies in association with structural crashworthiness involving crushing and fracture in ship-ship collisions. In the perspectives of multi-physics and multi-criteria involved, however, the nonlinear finite element method is certainly one of the most powerful techniques to model the problems. In a ship-ship collision accident where the bow of a striking ship is collided with the side of struck ship, the kinetic energy must be absorbed by both striking and struck ship structures in terms of collision damages and corresponding strain energies. As the bow structure of the striking ship is usually much stiffer than the side structure of the struck ship, the former has been modelled as a rigid body in the industry practice that does not allow deformation or damage so that no contribution to the energy absorption is made by the striking body. As the energy absorption characteristics of the striking ship depends on the structural arrangement of bulbous bow and flare, however, the contribution of striking ship cannot be entirely neglected. The aims of the present study are to examine the effects of a deformable striking ship structure on the structural crashworthiness of ship-ship collisions using LS-DYNA nonlinear finite element method computations. As an illustrative example in the paper, the struck ship is a VLCC class double hull oil tanker, while the struck ships are two types: a VLCC class tanker and a SUEZMAX class tanker. The relationships between collision forces versus penetration together with their energy absorption capabilities are characterized in association with the contributions of the striking ship bow where the deformable striking ship structures are compared with the rigid striking ship structures. Findings and insights developed from the present study are summarized. Details of the computations are documented.

Keywords: Ship-ship collision; deformable striking bow; oil tanker; structural crashworthiness; nonlinear finite element analysis.

1. Introduction

Accidental limit states (ALS) potentially brings about a catastrophe of serious injury or loss of life, environmental damage and loss of property or considerable expenditure of finance. The aim of ALS design is to ensure that the structure is able to bear up under specified accidental events such collision, grounding, fire and explosion and to enable evacuation of personnel from the structure for a sufficient period under specific environmental conditions after accidents occur (Paik and Thayamballi 2003, 2007).

Limit state design and safety assessment relevant to collisions and grounding are generally based on the energy absorption capability of the structure until accidental limit state is reached. As the energy absorption capability can be calculated by integration of the area below the reaction force versus

* Corresponding author. Tel.: +82-051-510-2429; fax: +82-051-518-7687.
E-mail address: jeompaik@pusan.ac.kr

penetration curve of the structure, the improving structural crashworthiness of the ships must be fulfilled to obtain the resultant force versus penetration relation of the structure in the accidental event.

As the amount of energy dissipation at the fore part of the striking ship is low comparatively than at the side part of the struck ship and **conservative** evaluations are relevant especially for safety designs in general, most ship collision simulations have been undertaken in the past where striking ships were modelled as a rigid body (Ammerman and Daidola 1996, Wisniewski and Kolakowski 2002, Haris and Amdahl 2011, Montewka et al. 2012, Sun et al. 2015, Zhang et al. 2016). On the other hand, some other studies have of course been conducted with striking ships that were modelled as a deformable body (Hogström and Ringsberg 2012, Haris and Amdahl 2013, Storheim and Amdahl 2015), but it is obvious that more efforts are recommended to examine the contribution of realistic striking ships to the structural crashworthiness of ship-ship collisions.

The aim of this study is to investigate the effects of a deformable striking-ship structure on the structural crashworthiness in ship-ship collisions. The characteristics of the energy absorption capabilities of ship structures in collision or grounding were studied in the literature by many investigators using the non-linear finite element method (Amdahl 1983, Simonsen 1997, Zhang 1999, Tornqvist 2003, Urban 2003, Alsos 2008, Hong 2009, Ehlers et al. 2010, 2016, Storheim and Amdahl 2015). This study also uses the non-linear finite element method with the LS-DYNA code (Hallquist 2010).

2. Collision Scenarios

Among various type of ships, oil tanker which can bring about a significant amount of pollution has been utilized as a target structure in the simulations and a host of researchers have fulfilled studies with oil tankers to reduce loss of financial properties and to prevent loss of lives and environmental damages in the literature (Zheng et al. 2007, Tavakoli et al. 2010, Kim et al. 2015, Faisal et al. 2016, Parunov et al. 2016, Youssef et al. 2014, 2017).

In the present study, it is considered that the side structure of a VLCC class double-hull oil tanker is collided with the bow structure of either a VLCC class double-hull oil tanker or a SUEZMAX class double-hull oil tanker. Tables 1 and 2 indicate the principal dimensions of the two types of ships. Figure 1 shows the finite element models of the entire hull structures for the two ships.

Table 1. Principal dimensions of the VLCC class double-hull hull oil tanker.

Parameter	Dimension
Overall length (m)	318.2
Moulded breadth (m)	60
Moulded depth (m)	30
Moulded draught (m)	21.6
Dead weight (ton)	300,000
Transverse frame spacing (m)	5.69

Table 2. Principal dimensions of the SUEZMAX class double-hull oil tanker.

Parameter	Dimension
Overall length (m)	272.0
Moulded breadth (m)	48.0
Moulded depth (m)	23.7
Moulded draught (m)	16.0
Dead weight (ton)	157,500
Transverse frame spacing (m)	4.8

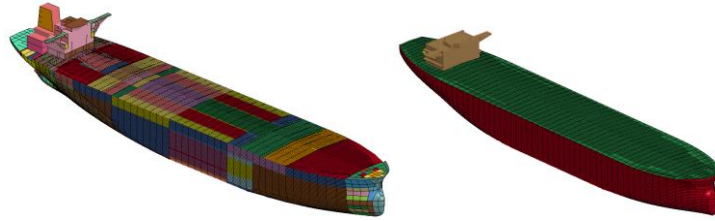


Figure 1. The VLCC class (left) and SUEZMAX class (right) double-hull oil tankers.

Collision scenarios considered in the present study are as follows:

- Case A: The side structure of the VLCC class double-hull oil tanker is struck by the bow structure of the VLCC class double-hull oil tanker
- Case B: The side structure of the VLCC class double-hull oil tanker is struck by the bow structure of the SUEZMAX class double-hull oil tanker

The colliding angle between the striking and struck ships as denoted in Figure 2 is varied in the present study at $\theta = 45, 90$ and 135 degrees. The speed of the striking ships is varied at $V_2 = 0.5, 3, 6$ and 10 knots, while the struck ship is standstill at $V_1 = 0$ knot. The location of collision is around midship (No. 3 cargo hold) of the struck ship. Also, it is considered that both striking and struck ships at the time of collision are in the laden (fully loaded) condition. Figure 3 shows the collision location for Cases A and B. Figure 4 shows the collision angle for Cases A and B. Table 3 indicates a summary for a total of 48 cases studied with varying the collision conditions considered in the present paper.

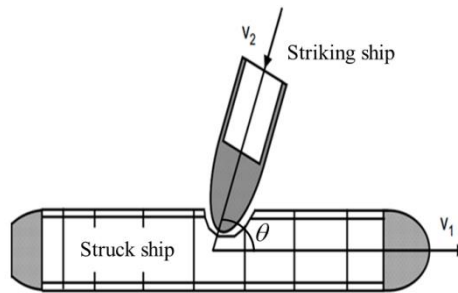


Figure 2. Definition of the collision angle between the striking and struck ships.

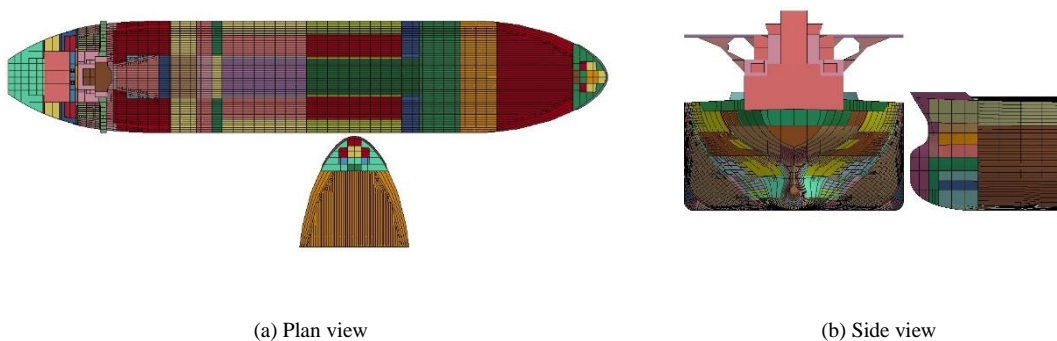


Figure 3(a). The collision location for the collision between the striking VLCC tanker and the struck VLCC tanker.

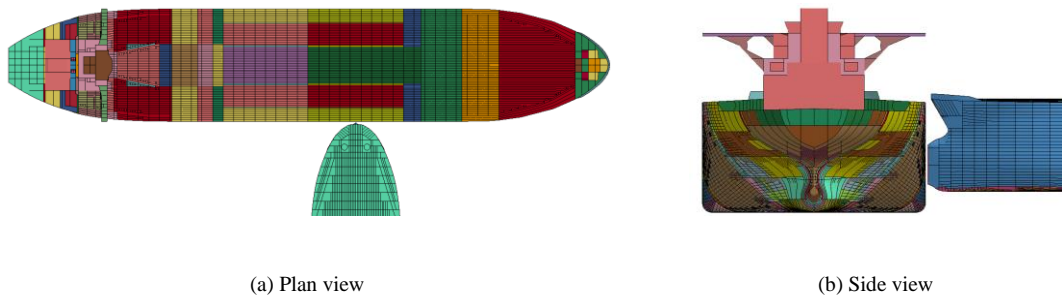


Figure 3(b). The collision location for the collision between the striking SUEZMAX tanker and the struck VLCC tanker.

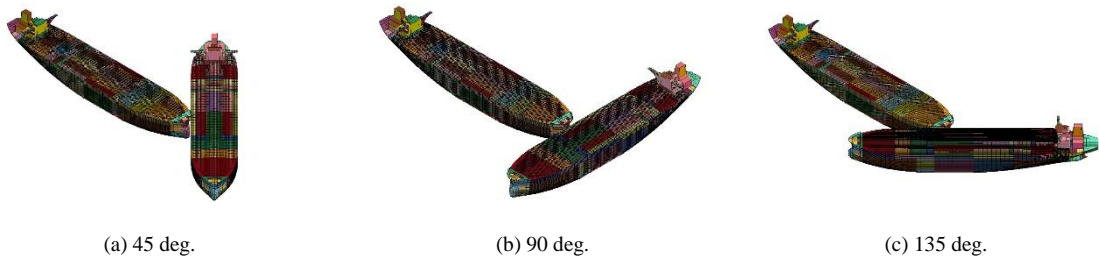


Figure 4(a). The collision angle for the collision between the striking VLCC tanker and the struck VLCC tanker.

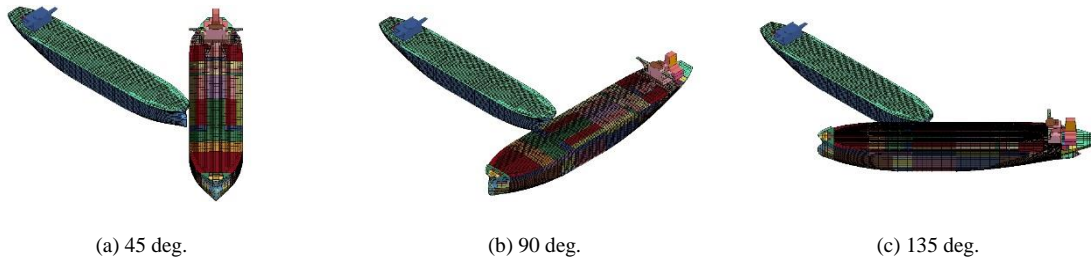


Figure 4(b). The collision angle for the collision between the striking SUEZMAX tanker and the struck VLCC tanker.

Table 3. Case study identification numbers with varying the collision conditions.

Case No.	Striking ship	Rigid or deformable	Collision angle θ (deg.)	Collision speed V_2 (knot)
1	VLCC	Rigid	90	0.5
2	VLCC	Rigid	90	3
3	VLCC	Rigid	90	6
4	VLCC	Rigid	90	10
5	VLCC	Rigid	45	0.5
6	VLCC	Rigid	45	3
7	VLCC	Rigid	45	6
8	VLCC	Rigid	45	10
9	VLCC	Rigid	135	0.5
10	VLCC	Rigid	135	3
11	VLCC	Rigid	135	6
12	VLCC	Rigid	135	10

13	VLCC	Deformable	90	0.5
14	VLCC	Deformable	90	3
15	VLCC	Deformable	90	6
16	VLCC	Deformable	90	10
17	VLCC	Deformable	45	0.5
18	VLCC	Deformable	45	3
19	VLCC	Deformable	45	6
20	VLCC	Deformable	45	10
21	VLCC	Deformable	135	0.5
22	VLCC	Deformable	135	3
23	VLCC	Deformable	135	6
24	VLCC	Deformable	135	10
25	SUEZMAX	Rigid	90	0.5
26	SUEZMAX	Rigid	90	3
27	SUEZMAX	Rigid	90	6
28	SUEZMAX	Rigid	90	10
29	SUEZMAX	Rigid	45	0.5
30	SUEZMAX	Rigid	45	3
31	SUEZMAX	Rigid	45	6
32	SUEZMAX	Rigid	45	10
33	SUEZMAX	Rigid	135	0.5
34	SUEZMAX	Rigid	135	3
35	SUEZMAX	Rigid	135	6
36	SUEZMAX	Rigid	135	10
37	SUEZMAX	Deformable	90	0.5
38	SUEZMAX	Deformable	90	3
39	SUEZMAX	Deformable	90	6
40	SUEZMAX	Deformable	90	10
41	SUEZMAX	Deformable	45	0.5
42	SUEZMAX	Deformable	45	3
43	SUEZMAX	Deformable	45	6
44	SUEZMAX	Deformable	45	10
45	SUEZMAX	Deformable	135	0.5
46	SUEZMAX	Deformable	135	3
47	SUEZMAX	Deformable	135	6
48	SUEZMAX	Deformable	135	10

3. Nonlinear Finite Element Method Modelling

3.1 Material Property Modelling

The striking and struck ship structures are made of both mild and high tensile steels. The mechanical properties of mild and high tensile steels are indicated in Table 4. In the present LS-DYNA simulations, the elastic-perfectly plastic material model was applied without considering the strain-hardening effect where the material option of “Piecewise Linear Plasticity” was adopted taking into account the dynamic effects (ISSC 2003, 2012, Sajdak and Brown 2004, Paik 2007a, 2007b, Yamada and Endo 2008).

Table 4. Material properties of the striking and struck ship structures.

Material property	Mild steel	High-tensile steel	
		AH32	AH36
Density, ρ (ton/m ³)	7.85	7.85	7.85
Young's modulus, E (MPa)	205,800	205,800	205,800
Poisson's ratio	0.3	0.3	0.3
Yield stress, σ_Y (MPa)	235	315	355
Cowper-Symonds coefficient	C	3200	3200
	q	5	5

3.2 Finite Element Size

As the structural crashworthiness in ship-ship collisions involves crushing and fracture, it is important to assign relevant mesh sizes in the finite element method modelling. In the present study, only plate-shell elements with an aspect ratio of almost unity were used but without beam elements. For the structural areas that are less affected by the collision, i.e., except for the cargo hold number 3 of the struck ship as well as the striking ship bow, coarse meshes were used in that plating was modelled by elements with about 1,000 mm in size and stiffener webs were modelled by one element while stiffener flanges were modelled by one element for an angle type or two elements for a T-type.

On the other hand, the collided areas were modelled by fine meshes. Paik and Thayamballi (2003, 2007) and Paik (2007a, 2007b) suggested techniques to define relevant size of finite elements to compute the structural crashworthiness of thin-walled structures when a rectangular type of plate-shell elements is utilized. The element size can then be determined from Equation (1) to represent the crushing behavior of thin walls as illustrated in Figure 5.

$$l_e \leq \frac{H}{8} = 0.983b^{2/3}t^{1/3} \quad (1)$$

where l_e is the element size, H is the half-fold length, b is the plate breadth between support members (e.g., stiffeners, frames, stringers), and t is the plate thickness.

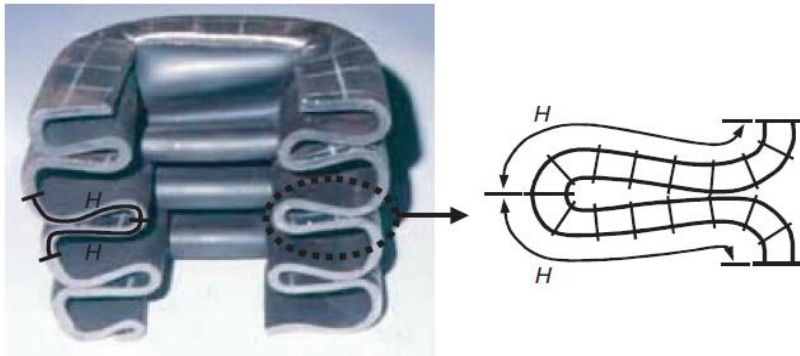


Figure 5. A thin-walled structure crushed under predominantly axial compression and cut at its midsection (Paik and Thayamballi 2007).

The above-mentioned Paik-Thayamballi method gives 200 - 250 mm for the element size. To reconfirm this value, a convergence study was performed by varying the element size. Figure 6 shows the results of the convergence study in terms of penetration and absorbed energy of the struck ship structures where Case A, i.e., the collision between a striking VLCC tanker and a struck VLCC tanker was considered with a collision angle of 90 deg. at a collision speed of 2 knots. Case B, i.e., the collision between a striking SUEZMAX tanker and a struck VLCC tanker was also studied and it was realized that the trend is quite similar. It is concluded from the convergence studies that the prediction

of the mesh size by the Paik-Thayamballi method is good enough as the element size was actually taken as 200 mm in the present study.

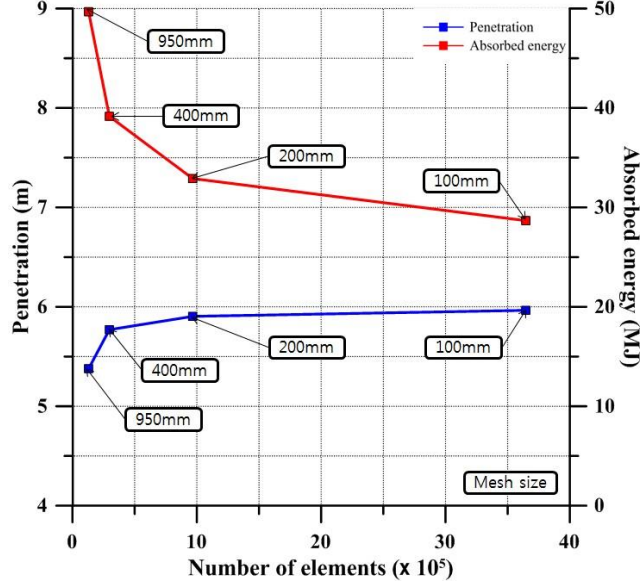


Figure 6. The convergence study to determine the element size.

3.3 Dynamic Yield Strength

The dynamic yield strength of material is determined from the Cowper-Symonds equation (2). The coefficients of Equation (2) are taken as indicated in Table 4, where it is noted that they differ for mild and high tensile steels (Paik 2007a, 2007b).

$$\sigma_{Yd} = \left[1 + \left(\frac{\dot{\varepsilon}}{C} \right)^{1/q} \right] \sigma_Y \quad (2)$$

where σ_Y and σ_{Yd} are the static and dynamic yield stresses, respectively, $\dot{\varepsilon}$ is the strain rate, and C and q are the Cowper-Symonds coefficients.

3.4 Dynamic Fracture Strain

In the present study, the dynamic fracture strain of material to be used for nonlinear finite element method computations is determined from the method developed by the authors (Ko et al. 2017). Figure 7 describes the method to determine the dynamic fracture strain where the static fracture strain ε_{fc} to be used for nonlinear finite element method computations is determined as a function of the static fracture strain ε_f of material determined from the tensile coupon test. The dynamic fracture strain to be used for nonlinear finite element method computations is then determined as an inverse of the Cowper-Symonds equation as indicated in Equation (3) (Paik and Thayamballi 2003, Paik 2007a, 2007b).

$$\varepsilon_{fd} = \left[1 + \left(\frac{\dot{\varepsilon}}{C} \right)^{1/q} \right]^{-1} \varepsilon_{fc} \quad (3)$$

where ε_{fc} and ε_{fd} are the static and dynamic fracture strains to be used for nonlinear finite element method computations, respectively, $\dot{\varepsilon}$ is the strain rate, and C and q are the Cowper-Symonds coefficients which are taken as indicated in Table 4.

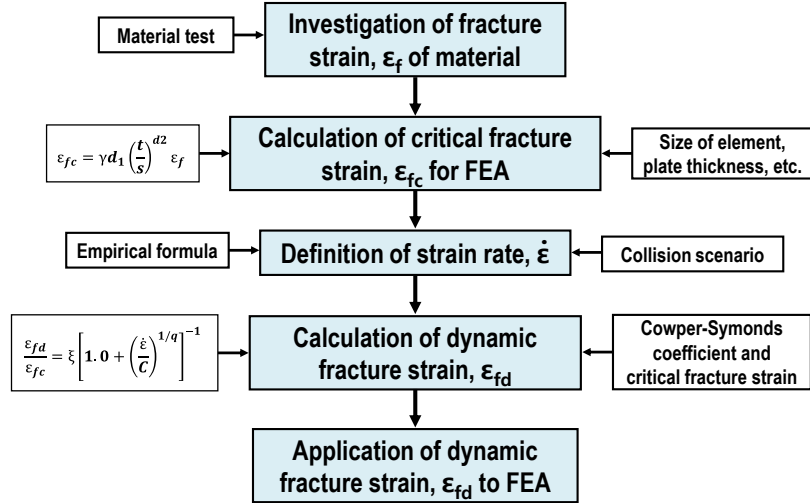


Figure 7. Procedure to determine the dynamic fracture strain to be used for nonlinear finite element method computations (Ko et al. 2017).

Upon using Equation (3), Ko et al. (2017) suggested to determine the strain rate $\dot{\epsilon}$ as a function of the collision speed as follows:

$$\dot{\epsilon} = 1.529V_2 - 0.686 \quad (4)$$

where V_2 is the collision speed in knot of the striking ship.

Table 5 indicates a summary of typical dynamic fracture strains determined from the above-mentioned method that are used for the nonlinear finite element method computations in the present study, although the plate thickness also affects the fracture strains and thus the dynamic fracture strains must differ for different plates with different thicknesses. However, it is interesting to note that the dynamic fracture strain is close to 0.1 which is well adopted in the industry practice, but it is seen that the method of Ko et al. (2017) gives a reasonable guidance to determine the dynamic fracture strains in general scenarios.

Table 5. The dynamic fracture strains used for the nonlinear finite element method computations.

Collision speed V_2 (knot)	Strain rate $\dot{\epsilon}$ (1/sec)	Steel grade	Static fracture strain ϵ_f	Critical fracture strain ϵ_{fc}	Dynamic fracture strain ϵ_{fd}	Dynamic yield stress σ_{yd}
0.5	0.079	Mild steel	0.42	0.126	0.098	302.416
		High tensile steel	0.38	0.114	0.102	352.692
3	3.901	Mild steel	0.42	0.126	0.078	382.240
		High tensile steel	0.38	0.114	0.090	397.322
6	8.488	Mild steel	0.42	0.126	0.073	407.010
		High tensile steel	0.38	0.114	0.087	411.170
10	14.604	Mild steel	0.42	0.126	0.069	426.728
		High tensile steel	0.38	0.114	0.085	422.195

3.5 Contact Problem Modelling

Thin-walled structural components can contact each other during crushing. Therefore, the structural crashworthiness analysis needs to model contact problems properly. Two types of contact problems are considered, i.e., general contact and self-contact. The former is affected by surfaces between different structural components, while the latter can arise by structural components themselves due to folding of crushing. Figure 8 illustrates some schematic representations of contact problems. Figure 9 shows an

example of the deformed shapes for thin-walled structures obtained from the structural crashworthiness analysis where the self-contact phenomenon is considered or not considered (Paik et al. 2009). Figure 10 shows the resultant forces or energy absorption capabilities with or without self-contact phenomenon (Paik et al. 2009). It is obvious that the effect of overlapping of contacted surfaces can be of significance. The effect of self-contact phenomenon is often omitted for saving computational times in simulations. In the present LS-DYNA computations, however, both general contact and self-contact are taken into account.

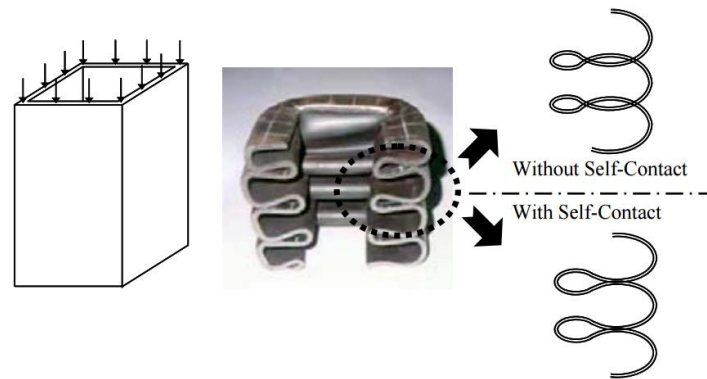
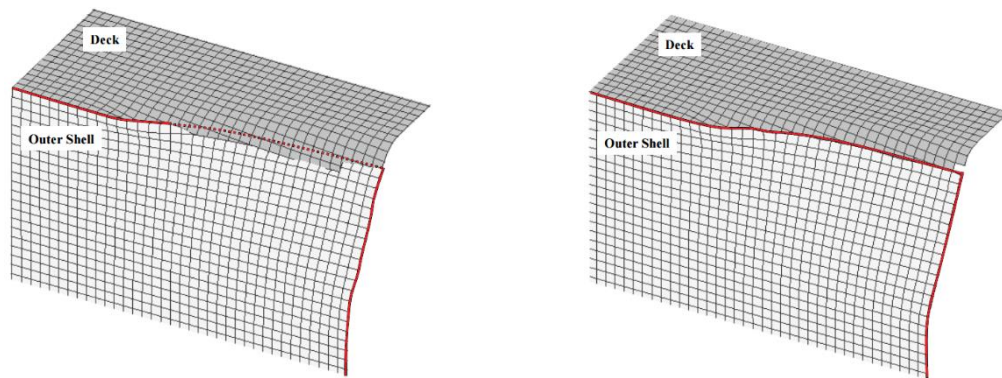


Figure 8. A schematic representation for crushing behavior with or without self-contact phenomenon (Paik et al. 2009).



(a) Deformed shape without self-contact phenomenon

(b) Deformed shape with self-contact phenomenon

Figure 9. Example of structural crashworthiness with or without self-contact phenomenon in terms of deformed shape (Paik et al. 2009).

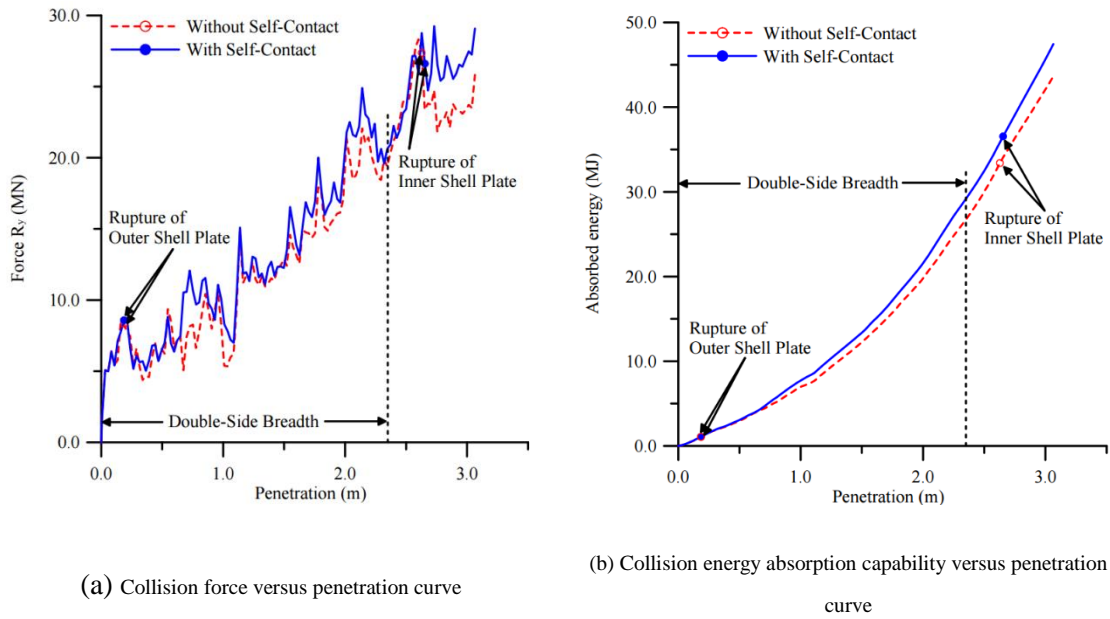


Figure 10. Example of structural crashworthiness with or without self-contact phenomenon in terms of resultant forces and energy absorption capabilities (Paik et al. 2009).

3.6 Friction Effect Modelling

While a structure undergoes an impact action with a striking body, the effect of friction may not be neglected if there is a relative velocity between the striking and struck bodies. The influence of friction may be of significance for a collision where the contact occurs at the side of the struck ship like a racking type (Paik and Thayamaballi 2007). In the present study, however, the friction constant was assumed as 0.3 for all cases of the studies. This is a simple assumption but it is to be noted that the characteristics of friction may change even at the same collision scenario as the penetration proceeds. In this regard, further studies are recommended.

3.7 Surrounding Water Effect Modelling

All vessels are on the ocean at the time of collision accidents, and thus striking and struck vessels are not fixed in any direction where they naturally move even after collisions. In addition, the effect of sea water (e.g., added mass) against ship's motions cannot be neglected as part of kinetic energy can be consumed for the movement of the ships involved.

In the present nonlinear finite element method computations, free body boundary condition (without displacement and rotational restrictions) of ships is applied by using LS-DYNA/MCOL program which can simulate a ship motion taking into account the effect of the added mass after collision (Kuroiwa et al. 1995, Kuroiwa 1996, Kitamura 2000, Le Source et al. 2003). Figure 11 illustrates the LS-DYNA/MCOL collision simulation system (Ferry et al. 2002).

In this modelling, the effect of surrounding water is taken into account in terms of hydrodynamic forces associated with the deceleration of the ships where a virtual mass of the striking and struck ships in surge, sway and yaw motions is added to the actual ship mass. The motions of pitch, roll and heave may be neglected because these motion components are minimal with regard to the energy translated into these three degrees of freedom, compared to the motion components in the surge, sway, and yaw directions.

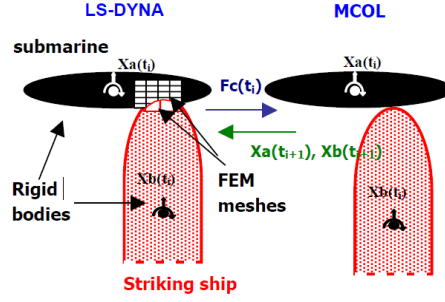


Figure 11. Boundary system in LS-DYNA/MCOL collision simulation (Ferry et al. 2002).

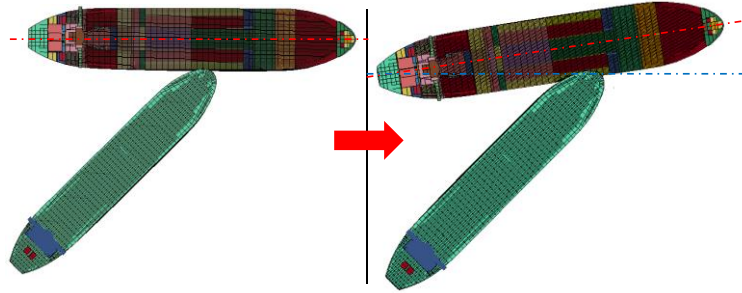


Figure 12. Motion of struck ship before (left) and after (right) collision in LS-DYNA/MCOL simulations.

Upon using the LS-DYNA/MCOL solver for ship-ship collisions, the resultant forces and moments imposed on the struck ship structure are calculated at each time step during the simulation, and by using these values the new position of the struck ship is then updated without additional boundary conditions as shown in Figure 12. In the present computations, $c_{11} = 0.05$, $c_{22} = 0.85$, and $c_{33} = 0.21$ in Equation (4) are taken for the movements of the struck ship at each direction (Pedersen and Zhang 1998).

$$a_{11} = c_{11}m_2, \quad a_{22} = c_{22}m_2, \quad a_{33} = c_{33}I_2 \quad (5)$$

where a_{11} , a_{22} and a_{33} are the add masses in the direction of surge, sway and yaw motions, respectively, c_{11} , c_{22} and c_{33} are the coefficients of add masses for each motion, m_2 is the mass of struck vessel, and I_2 is the mass moment of inertia of struck vessel.

4. Results and Discussions

In the present study, LS-DYNA computations have been performed for each of 48 cases addressed in Table 3 until the applied kinetic energy has been entirely consumed as per the corresponding collision scenario. Various results are obtained including deformations, stresses, and resultant forces of both striking and struck ship structures. The relationships between resultant forces versus time, and between penetration versus time are first identified from the computations. The relationships between resultant forces versus penetration are then obtained from the two relationships, namely resultant forces-time relation and penetration-time relation, where resultants forces and penetration are taken at the identical time each other. The relationships between absorbed energy versus penetration can then be obtained by integrating the areas below the corresponding curves.

Maximum penetration is one of primary concerns as the bow structure of striking ship penetrates the side structure of struck ship. In the present study, reference penetration of side or bow structures was measured for the maximum sideways penetration of struck ship's cargo hold number 3 or for the maximum deformation of striking ship's bulbous bow tip along the ship's longitudinal direction. Table 6 indicates a summary of maximum penetration together with the corresponding maximum resultant forces and absorbed energy amount until the kinetic energy is entirely consumed.

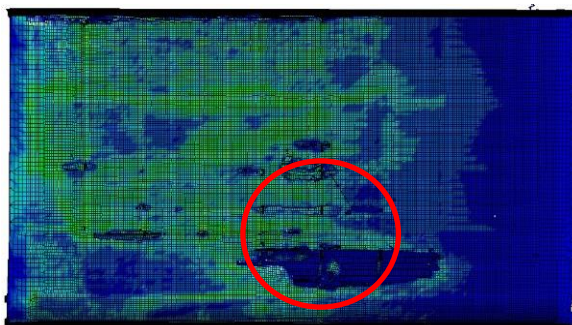
Table 5. Maximum structural consequence stems from collisions.

Case	Collision angle θ (deg.)	Collision speed V_2 (knot)	Max. penetration (m)	Max. absorbed energy (MJ)	Max. resultant force (MN)
1	90	0.5	0.19	2.60	8.29
2	90	3	3.73	61.02	30.70
3	90	6	8.70	220.55	36.40
4	90	10	20.82	485.09	45.39
5	45	0.5	0.08	0.31	3.74
6	45	3	1.23	19.91	23.07
7	45	6	2.76	102.35	40.86
8	45	10	3.63	322.84	61.04
9	135	0.5	0.06	0.27	3.70
10	135	3	1.46	18.75	21.63
11	135	6	2.36	167.55	39.45
12	135	10	17.11	644.91	56.17
13	90	0.5	0.18	2.41	8.07
14	90	3	3.00	32.87	25.47
15	90	6	4.75	131.71	47.05
16	90	10	7.00	342.58	61.97
17	45	0.5	0.10	0.24	1.76
18	45	3	0.14	8.25	29.73
19	45	6	0.51	44.19	47.21
20	45	10	1.66	117.29	61.24
21	135	0.5	0.09	0.24	1.69
22	135	3	0.08	10.00	22.70
23	135	6	0.31	44.42	45.84
24	135	10	2.24	170.34	57.24
25	90	0.5	0.13	2.02	9.48
26	90	3	3.45	50.62	30.02
27	90	6	8.14	175.01	33.89
28	90	10	21.68	412.25	35.19
29	45	0.5	0.00	0.01	0.88
30	45	3	0.44	9.75	15.20
31	45	6	0.97	82.05	26.47
32	45	10	3.75	291.21	45.89
33	135	0.5	0.00	0.00	1.09
34	135	3	0.21	9.22	15.81
35	135	6	2.96	122.12	26.98
36	135	10	10.65	402.42	44.93
37	90	0.5	0.14	1.97	9.42
38	90	3	3.09	42.72	29.12
39	90	6	6.77	154.80	35.64
40	90	10	16.31	345.73	40.52
41	45	0.5	0.01	0.04	2.20

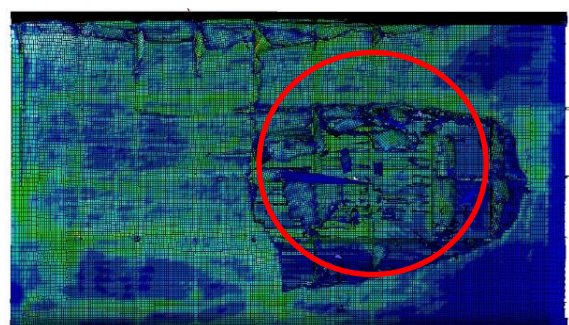
42	45	3	1.01	12.26	24.68
43	45	6	1.94	84.70	38.39
44	45	10	3.27	313.53	55.03
45	135	0.5	0.01	0.02	2.16
46	135	3	1.25	10.00	22.70
47	135	6	2.22	87.45	39.32
48	135	10	5.33	303.58	50.82

Figures 13 and 14 show deformed shapes of the VLCC tanker structures struck by the VLCC or by the SUEZMAX tanker structures with a deformable or rigid bow, where collision angles are varied while the collision speed was fixed at 10 knots. The deformations of side structures were measured at around the tip of the striking bow. It is obvious that the damage extent and amount of side structures struck by a rigid striking bow are much larger than those struck by a deformable striking bow. **The collision damage location and extent are associated with the distribution of absorbed energy between the striking and struck ships. The areas exposed to the impact loading change with time depending on the characteristics of the striking and struck ships) and thus the most damaged areas also differ in different collision cases.** Figures 15 and 16 show the relationships between resultant forces or absorbed energies versus penetration in conjunction with Figures 13 and 14. It is found that the differences between the deformable and rigid bows are of significance in terms of the structural crashworthiness associated with outer or inner hull rupture and maximum penetration. Considering that the deformable bow model is more realistic and accurate, it is recommended that the rigid striking bow model applied in the current industry practice should not be used for more refined computations of the structural crashworthiness of ship-ship collisions.

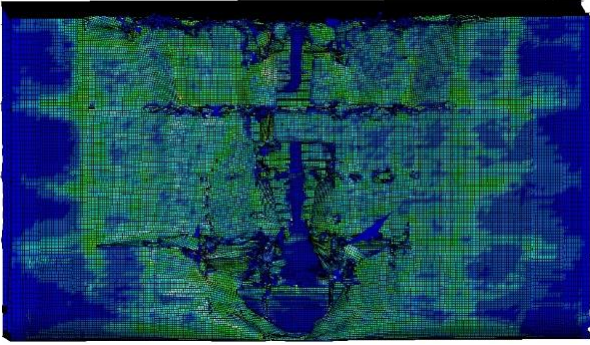
Figures 17 and 18 show the behavior of penetration or resultant forces with time for the striking VLCC or SUEZMAX tanker. Figures 19 and 20 show the effects of the deformable striking ship bow on the maximum penetration, maximum absorbed energy and maximum resultant forces with varying angle or speed of collision. It is found from these results that the effects of the deformable striking ship bow are of significance as the collision speed increases. **It is obvious from these figures that the effects of a deformable striking bow become more significant at a faster collision speed.** Also, the maximum penetration occurs at the collision angle of 90 deg. It is noted that the penetration tends to be greater by the striking SUEZMAX tanker than by the striking VLCC tanker regardless of the fact that the displacement of the latter ship is larger than the former ship. This is because the bulbous bow of the former ship is sharper than that of the latter ship. It is again obvious from these computations that the deformable striking ship bow structures absorb some part of the initial kinetic energy of the collision as they penetrate into the struck ship structures in contrast to the industry practice where all of the initial kinetic energy is considered to be absorbed by the struck ship structures only because the striking ship bow is modeled as a rigid body.



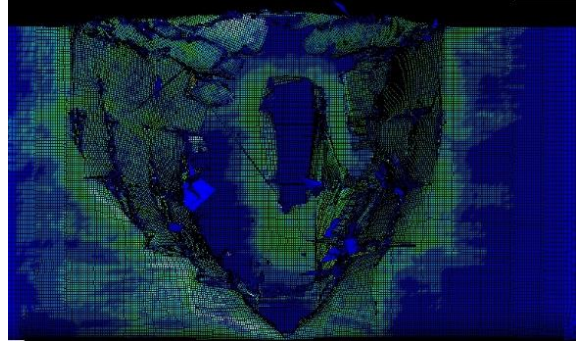
(a) Deformable bow at a collision angle of 45 deg.



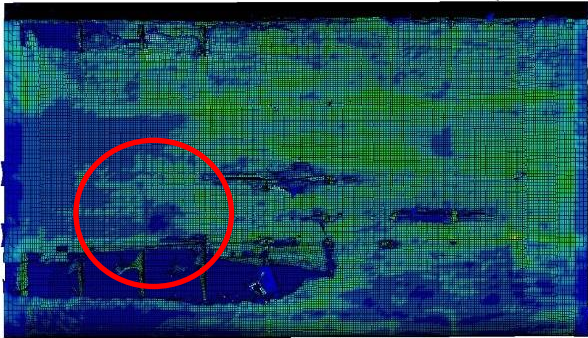
(b) Rigid bow at a collision angle of 45 deg.



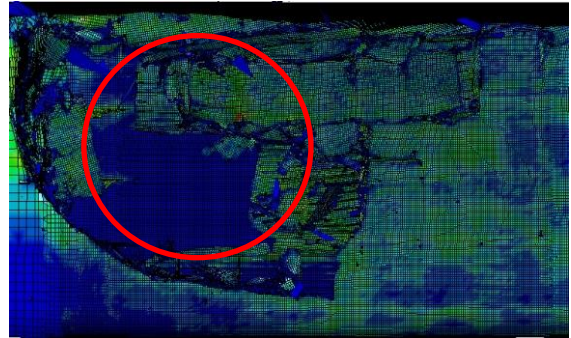
(c) Deformable bow at a collision angle of 90 deg.



(d) Rigid bow at a collision angle of 90 deg.

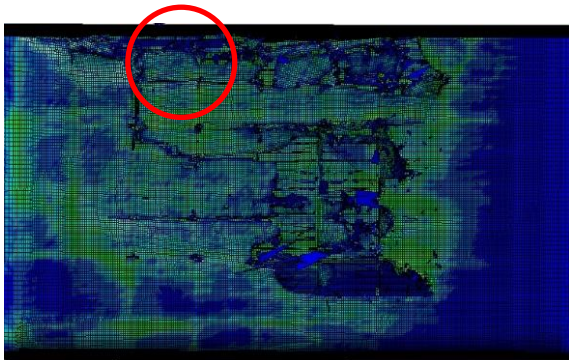


(e) Deformable bow at a collision angle of 135 deg.

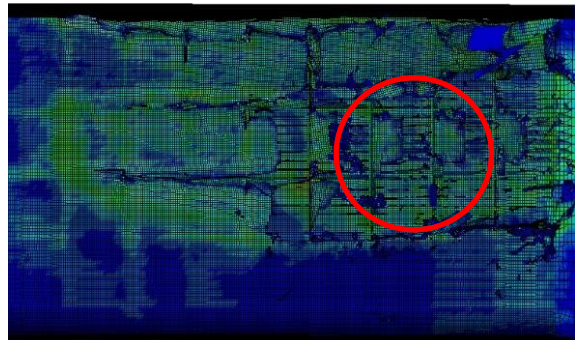


(f) Rigid bow at a collision angle of 135 deg.

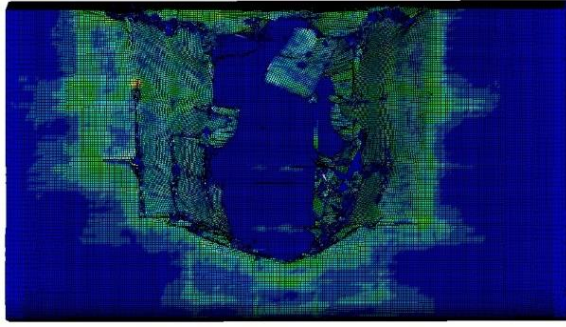
Figure 13. Deformed shapes of struck VLCC tanker at around the tip of striking VLCC bow with a collision speed of 10 knots.



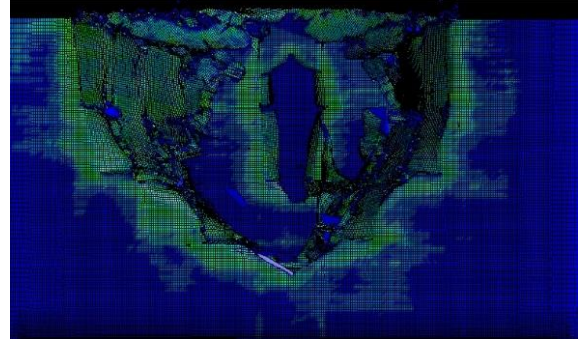
(a) Deformable bow at a collision angle of 45 deg.



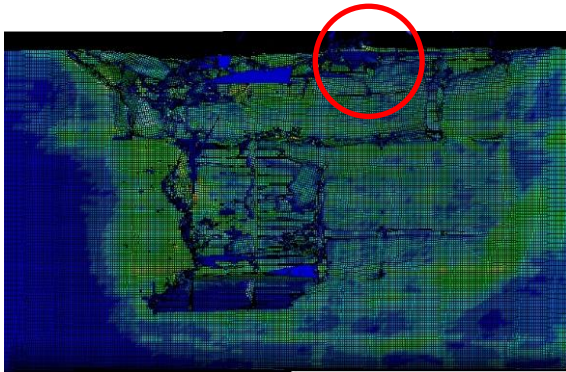
(b) Rigid bow at a collision angle of 45 deg.



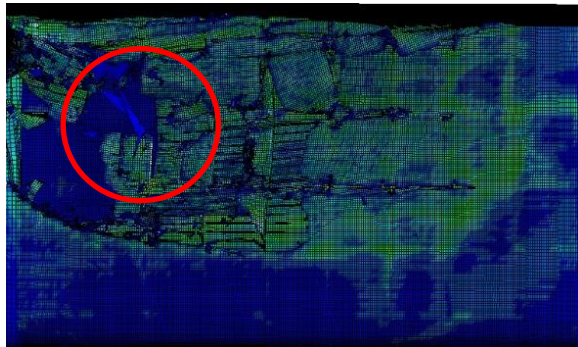
(c) Deformable bow at a collision angle of 90 deg.



(d) Rigid bow at a collision angle of 90 deg.

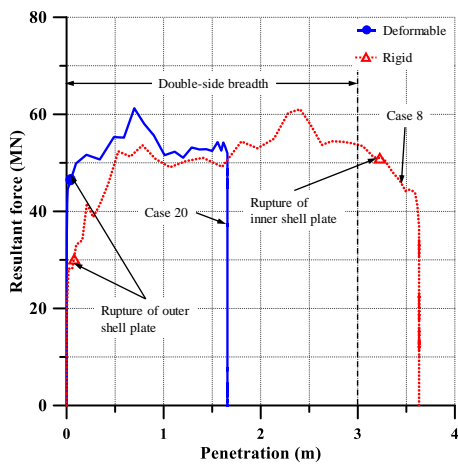


(e) Deformable bow at a collision angle of 135 deg.

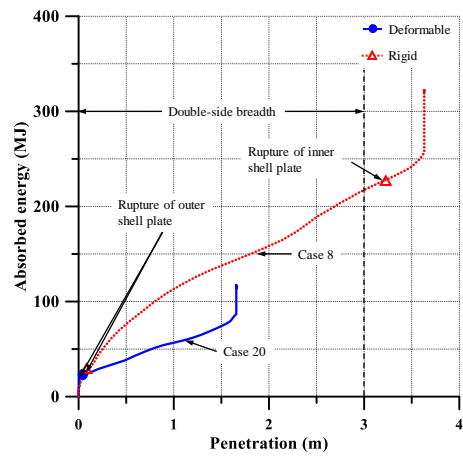


(f) Rigid bow at a collision angle of 135 deg.

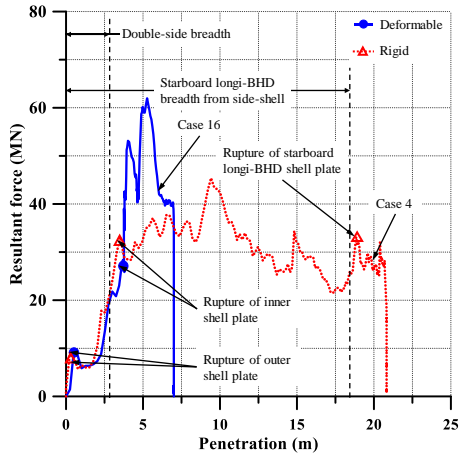
Figure 14. Deformed shapes of struck VLCC tanker at around the tip of striking SUEXMAX bow with a collision speed of 10 knots.



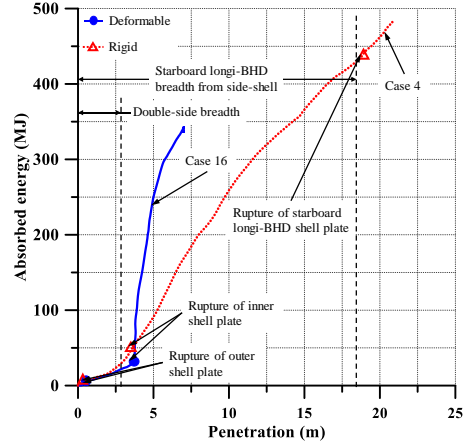
(a) Collision angle of 45 deg.



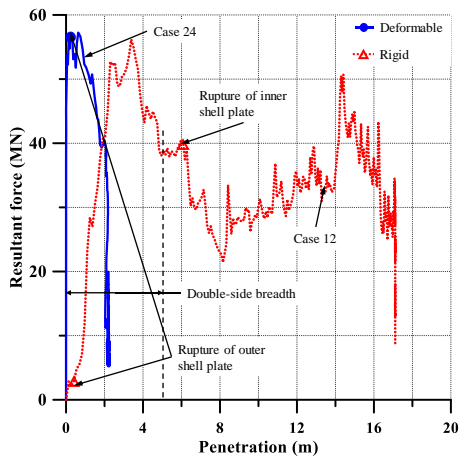
(b) Collision angle of 45 deg.



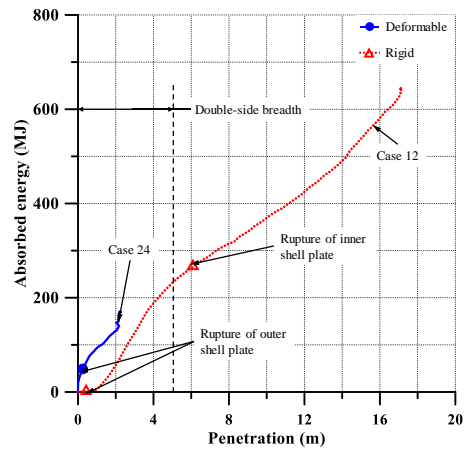
(c) Collision angle of 90 deg.



(d) Collision angle of 90 deg.

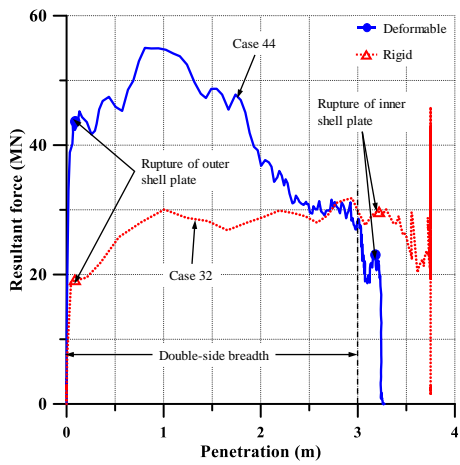


(e) Collision angle of 135 deg.

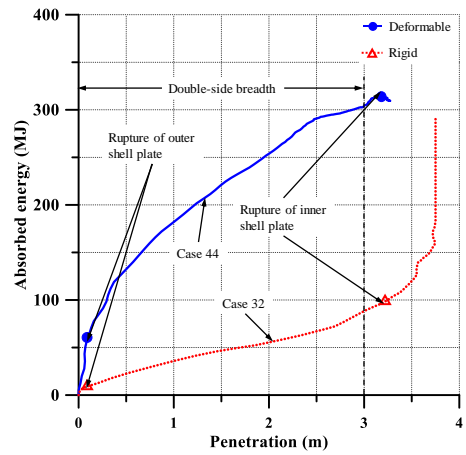


(f) Collision angle of 135 deg.

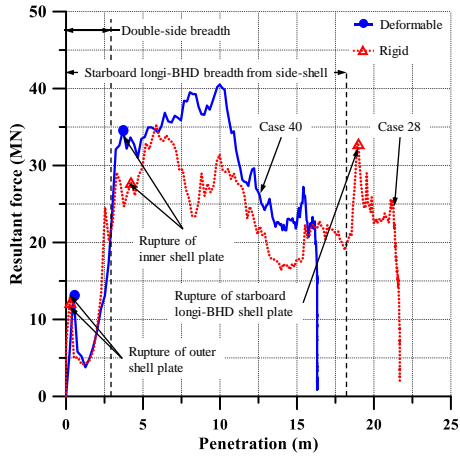
Figure 15. The relationships between resultant forces or absorbed energies versus penetration for the VLCC tanker struck by the VLCC tanker at a collision speed of 10 knots.



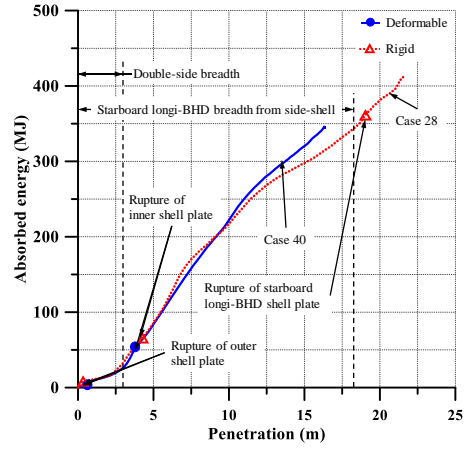
(a) Collision angle of 45 deg.



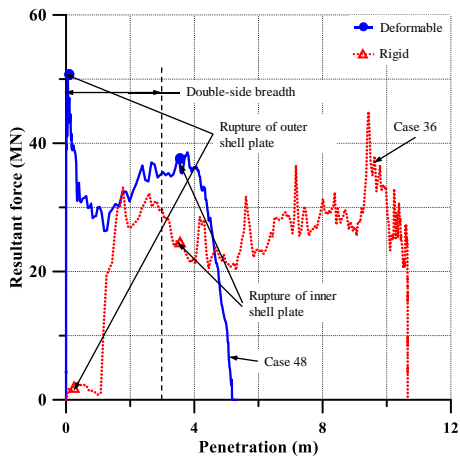
(b) Collision angle of 45 deg.



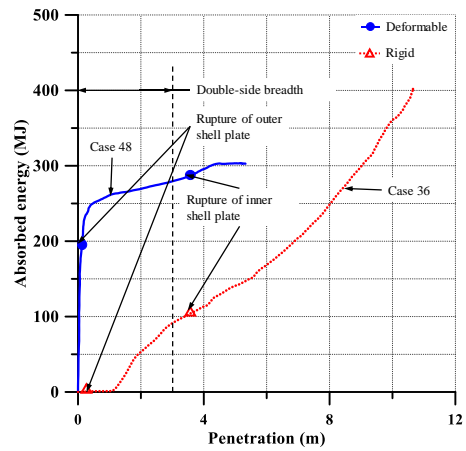
(c) Collision angle of 90 deg.



(d) Collision angle of 90 deg.

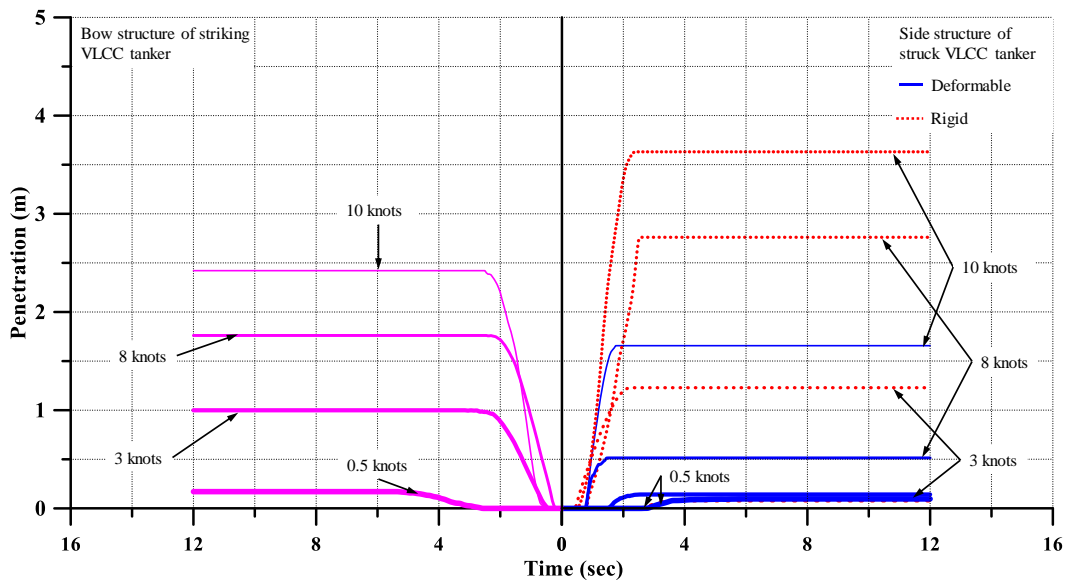


(e) Collision angle of 135 deg.

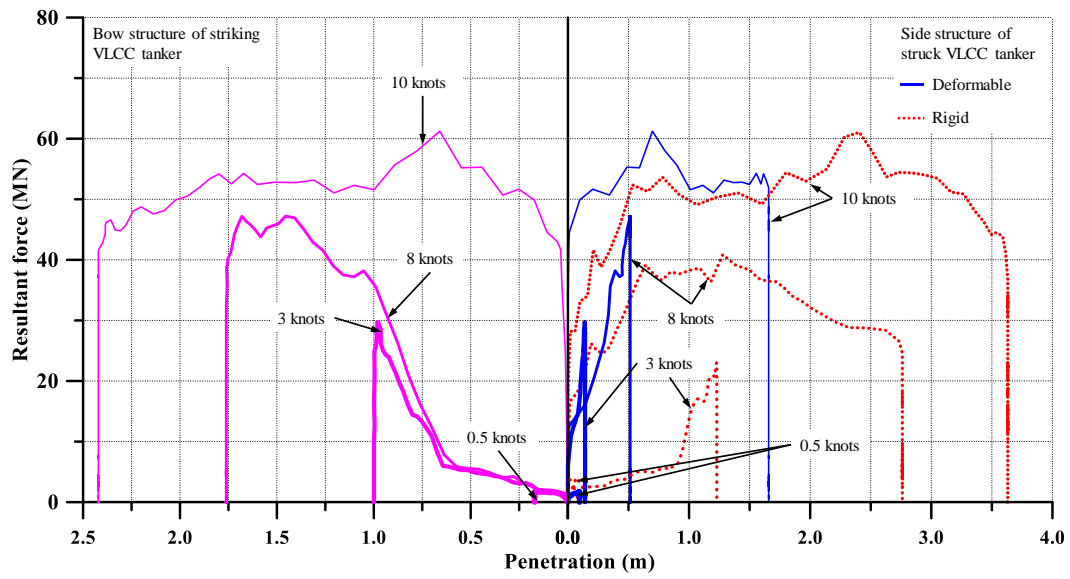


(f) Collision angle of 135 deg.

Figure 16. The relationships between resultant forces or absorbed energies versus penetration for the VLCC tanker struck by the SUEZMAX tanker at a collision speed of 10 knots.

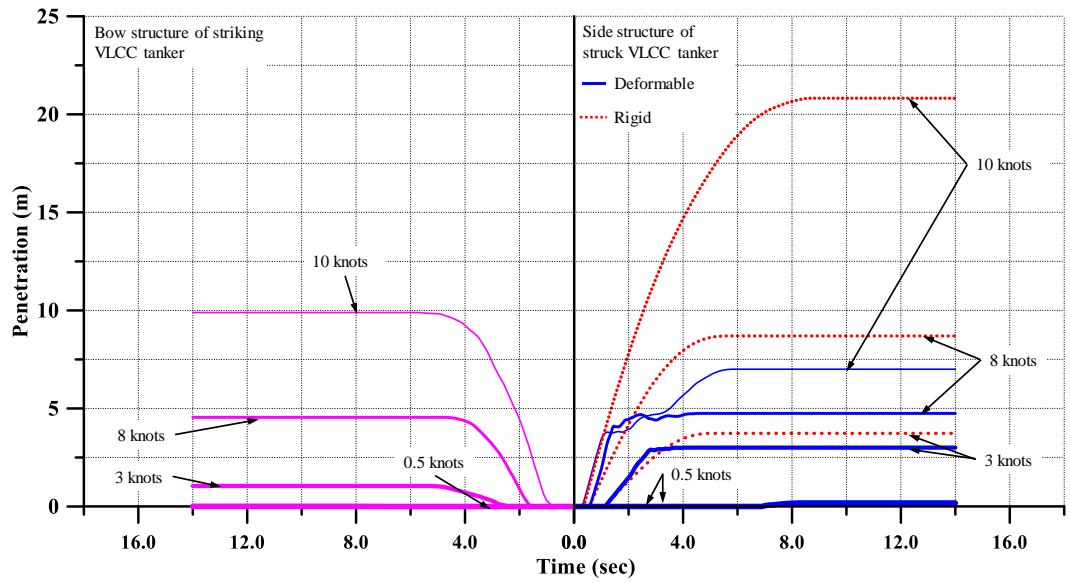


(a) The behavior of penetration with time

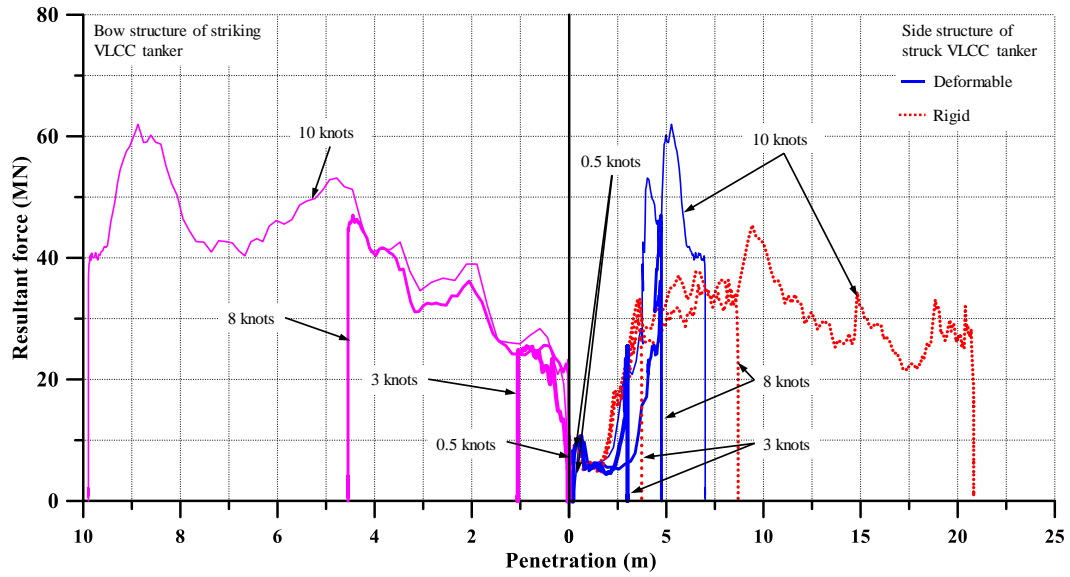


(b) The behavior of resultant forces with time

Figure 17(a). The effects of the deformable striking VLCC tanker at a collision angle of 45 deg.

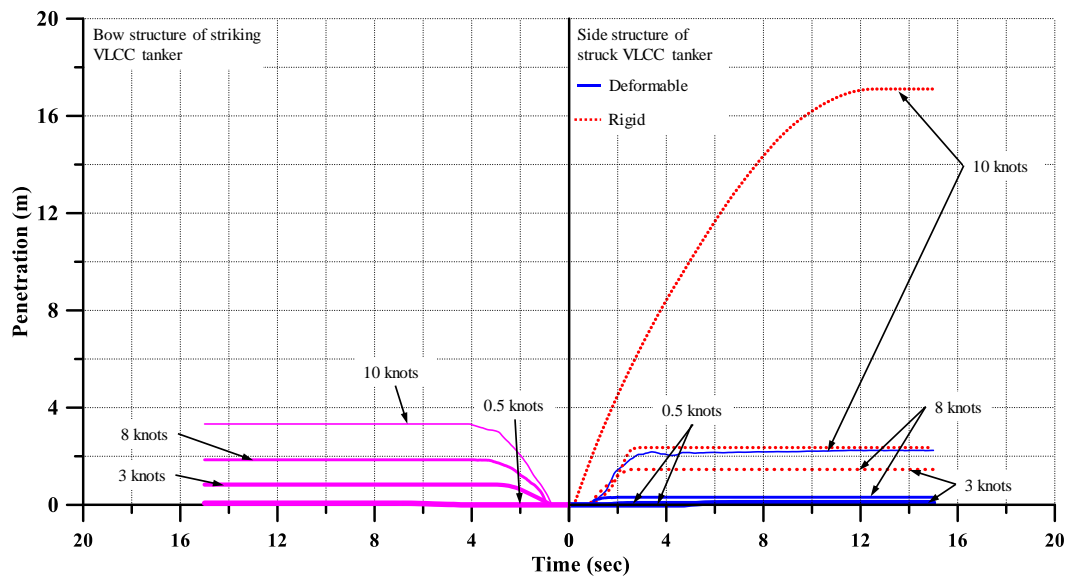


(a) The behavior of penetration with time

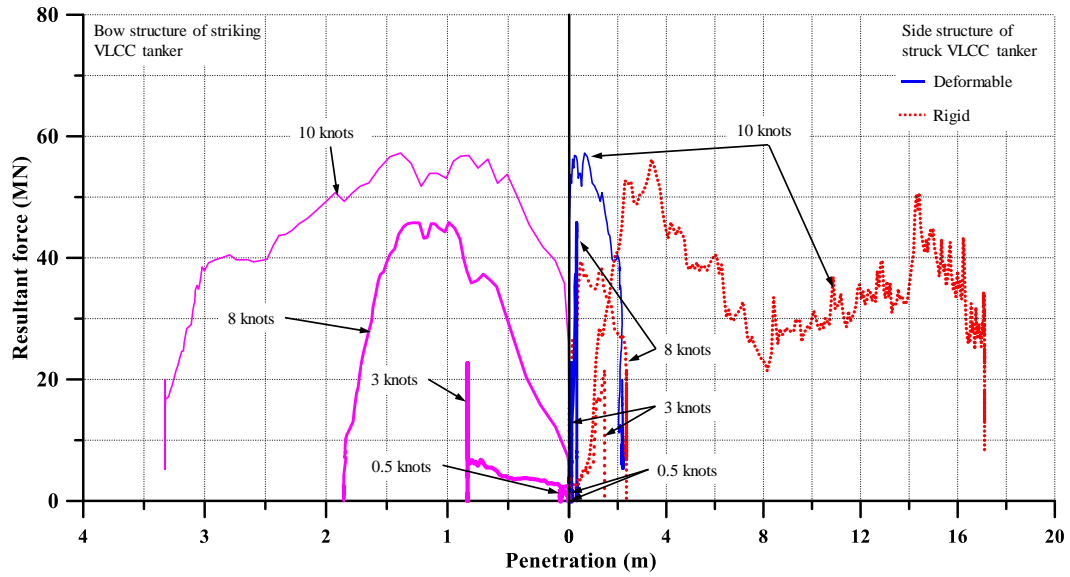


(b) The behavior of resultant forces with time

Figure 17(b). The effects of the deformable striking VLCC tanker at a collision angle of 90 deg.

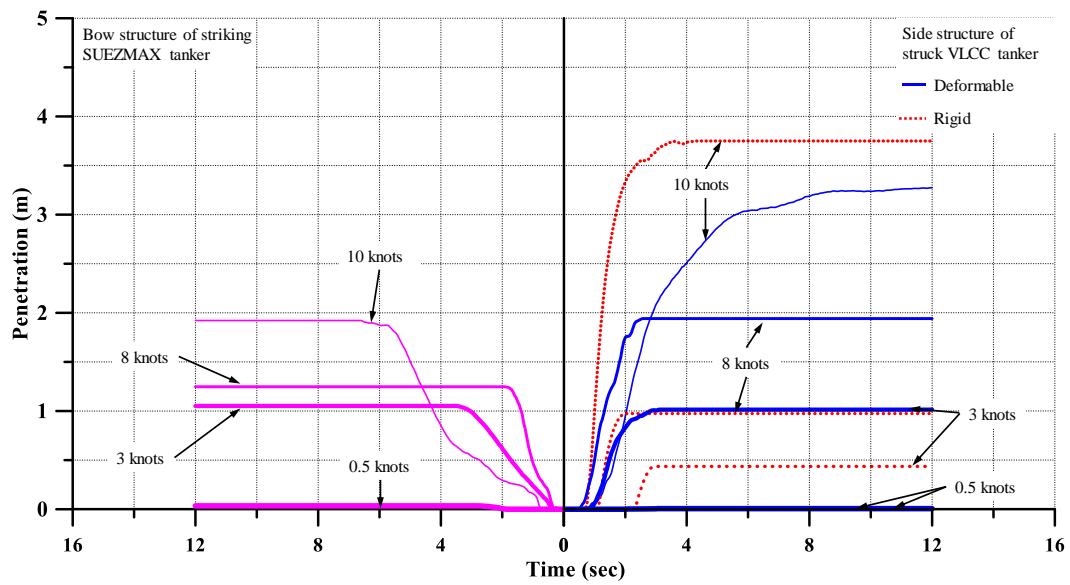


(a) The behavior of penetration with time

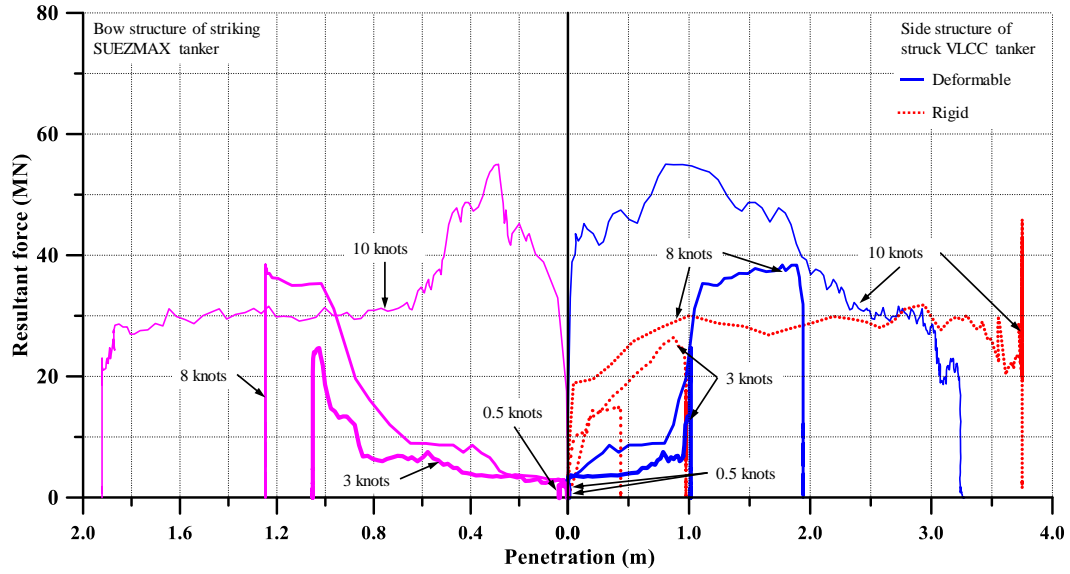


(b) The behavior of resultant forces with time

Figure 17(c). The effects of the deformable striking VLCC tanker at a collision angle of 135 deg.

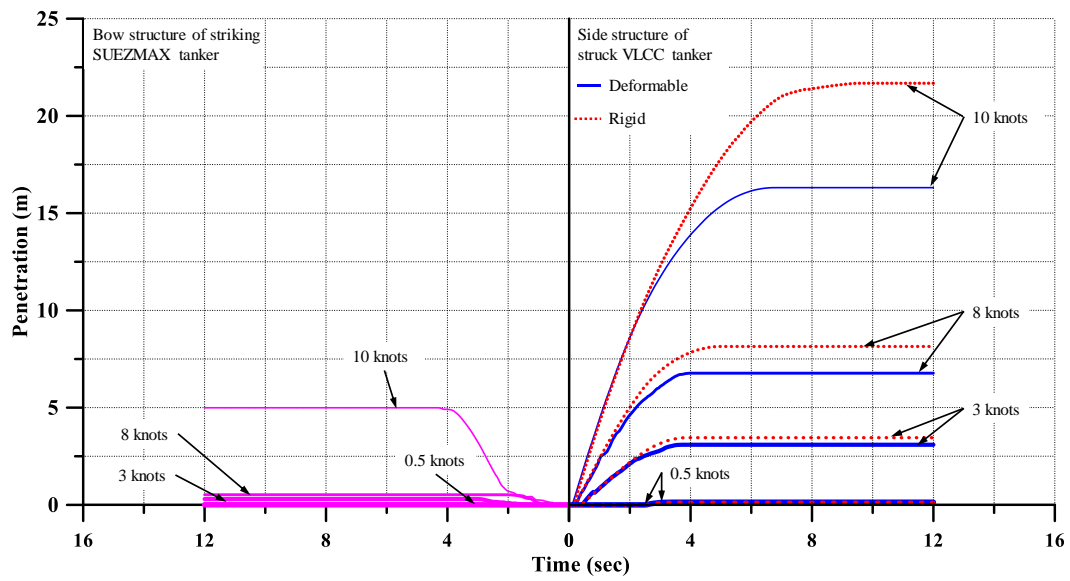


(a) The behavior of penetration with time

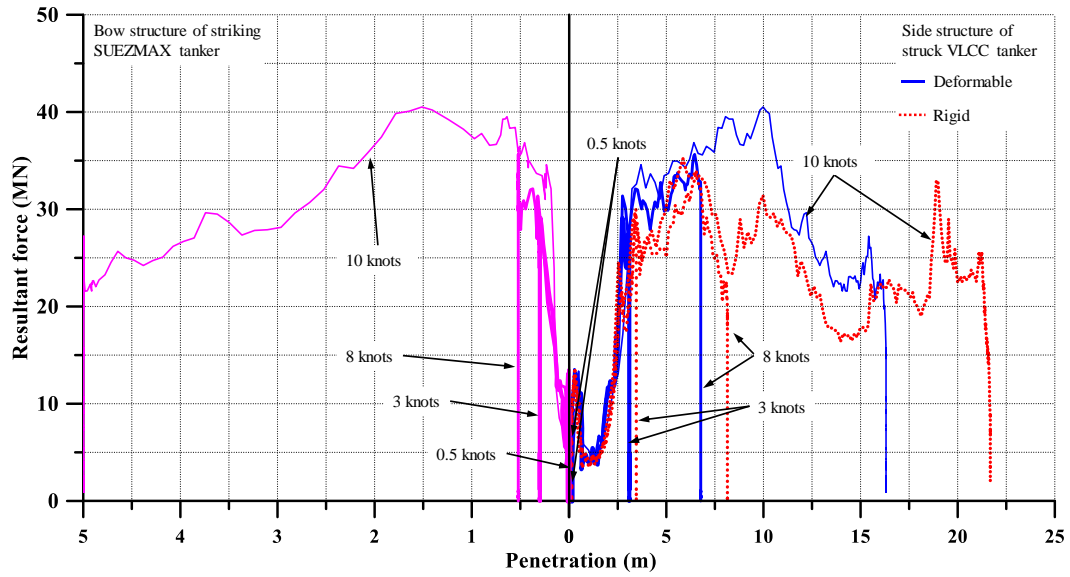


(b) The behavior of resultant forces with time

Figure 18(a). The effects of the deformable striking SUEZMAX tanker at a collision angle of 45 deg.

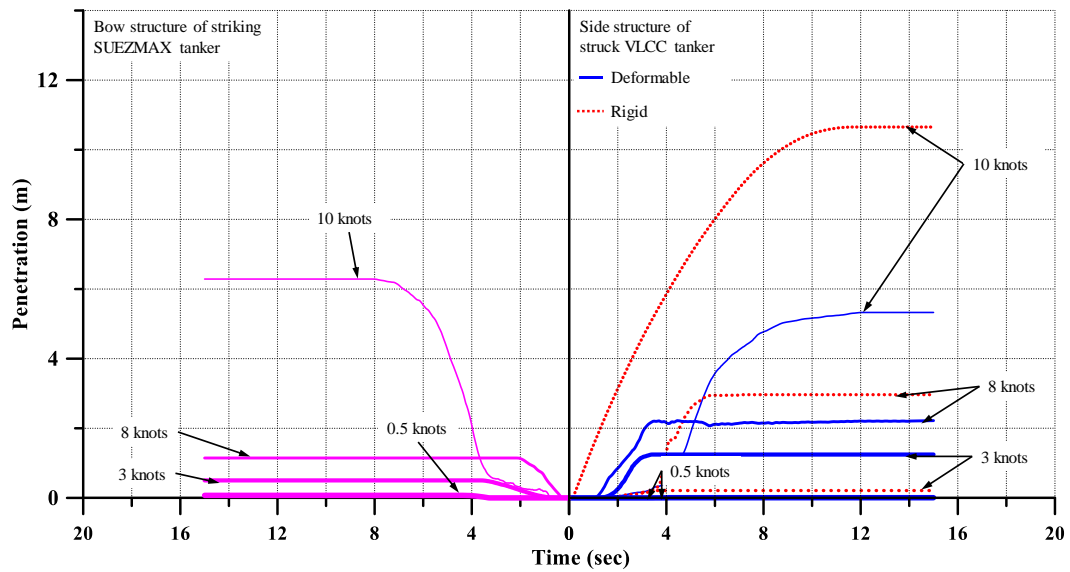


(a) The behavior of penetration with time

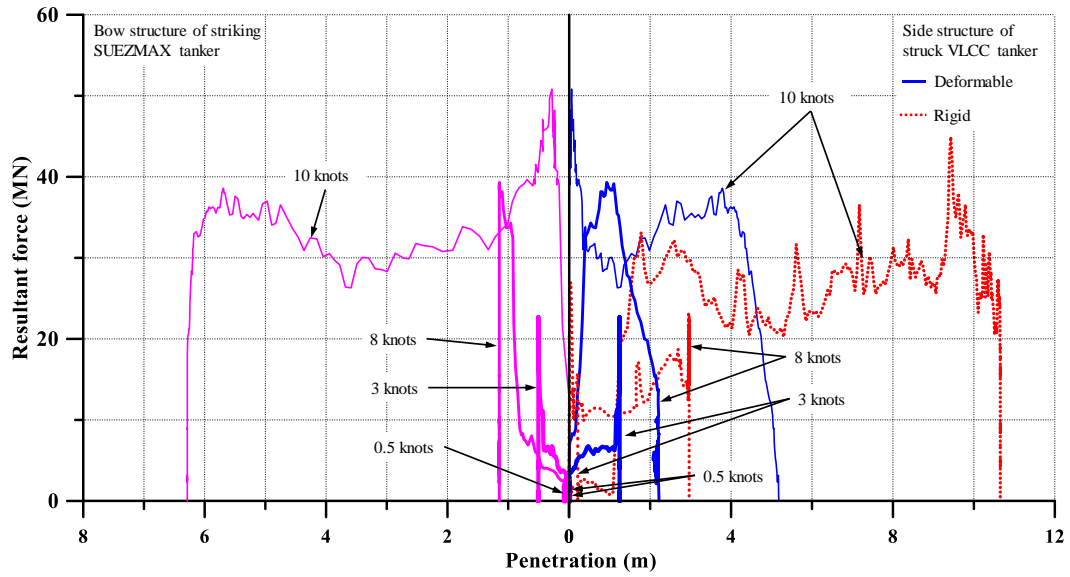


(b) The behavior of resultant forces with time

Figure 18(b). The effects of the deformable striking SUEZMAX tanker at a collision angle of 90 deg.

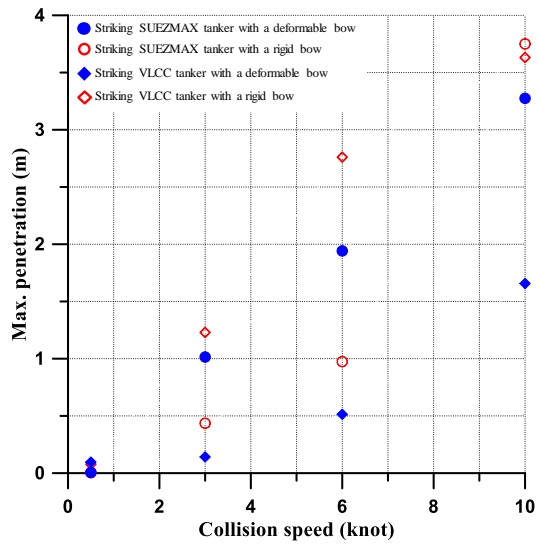


(a) The behavior of penetration with time

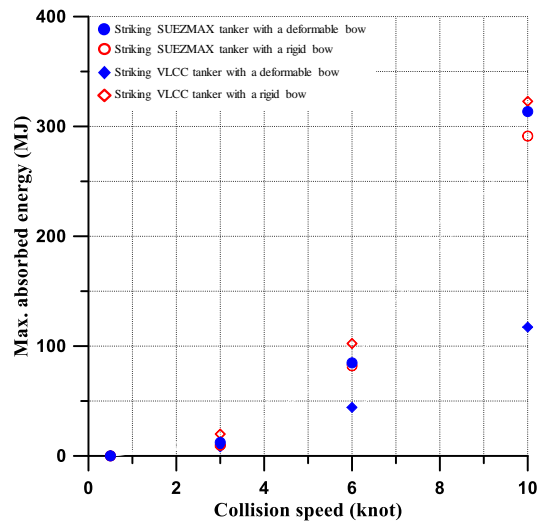


(b) The behavior of resultant forces with time

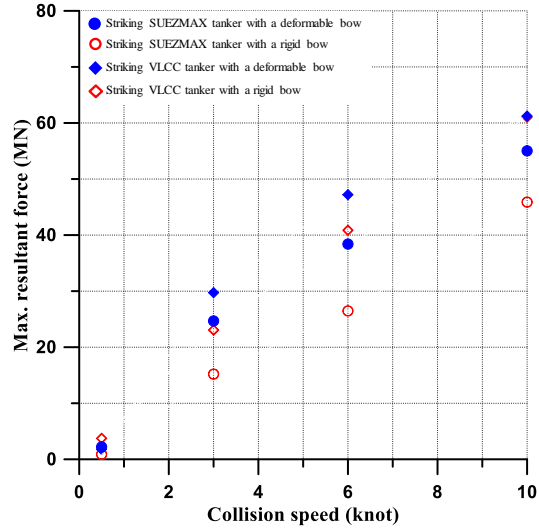
Figure 18(c). The effects of the deformable striking SUEZMAX tanker at a collision angle of 135 deg.



(a)

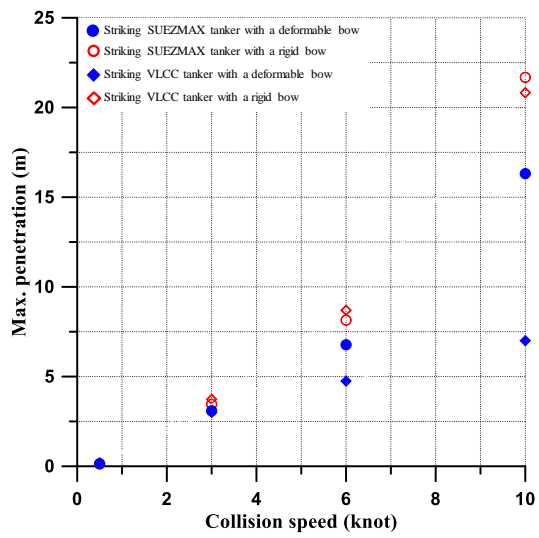


(b)

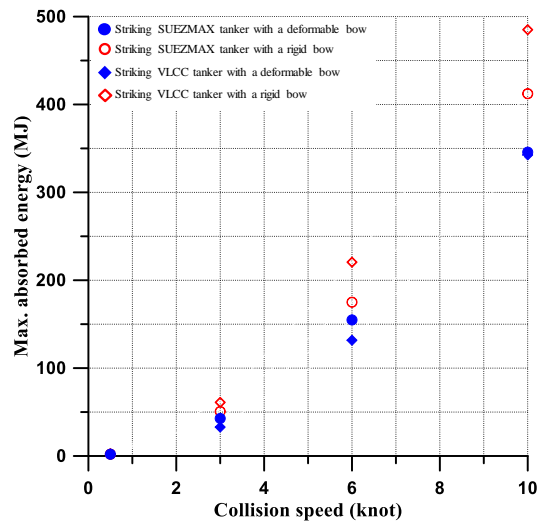


(c)

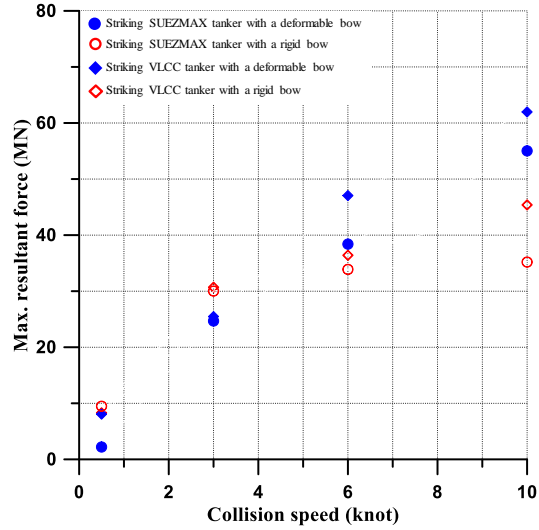
Figure 19(a). The effects of the deformable striking ship bow on the maximum penetration, maximum absorbed energy and maximum resultant force at a collision angle of 45 deg.



(a)

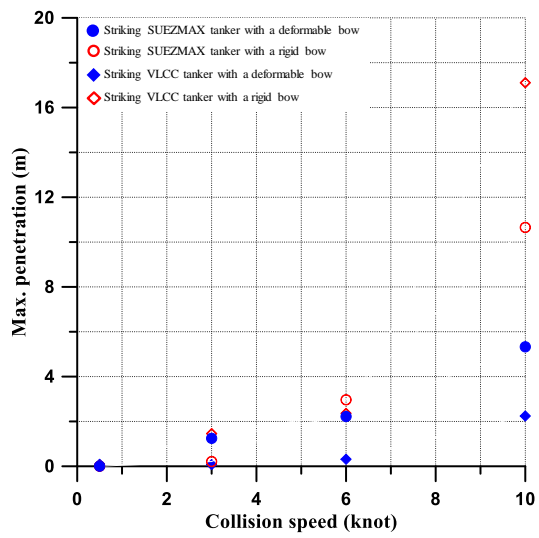


(b)

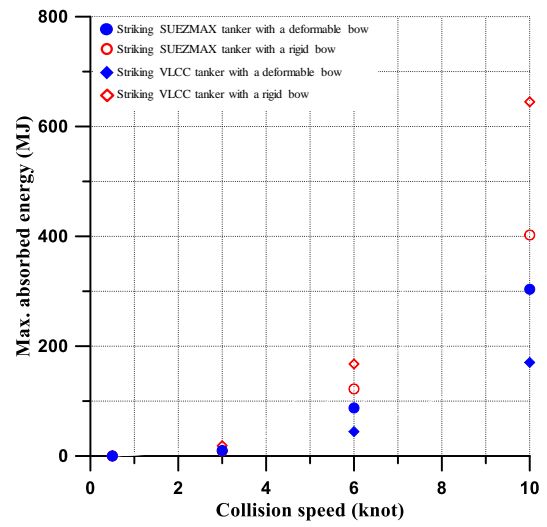


(c)

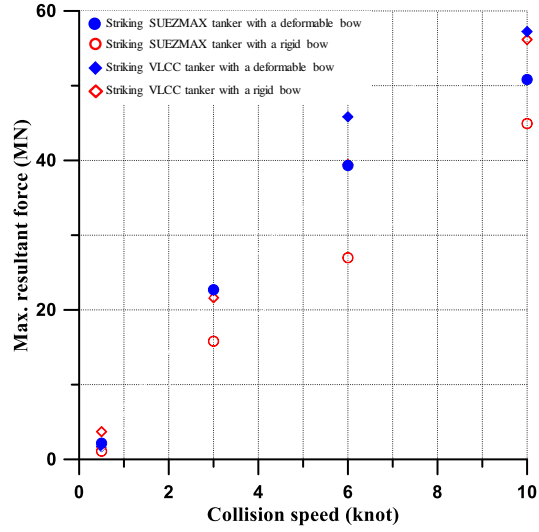
Figure 19(b). The effects of the deformable striking ship bow on the maximum penetration, maximum absorbed energy and maximum resultant force at a collision angle of 90 deg.



(a)

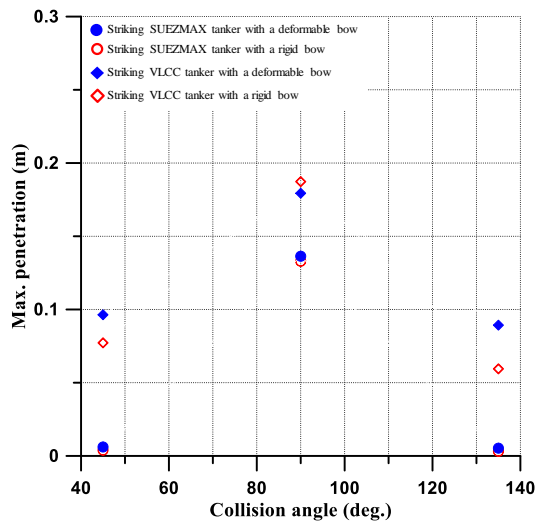


(b)

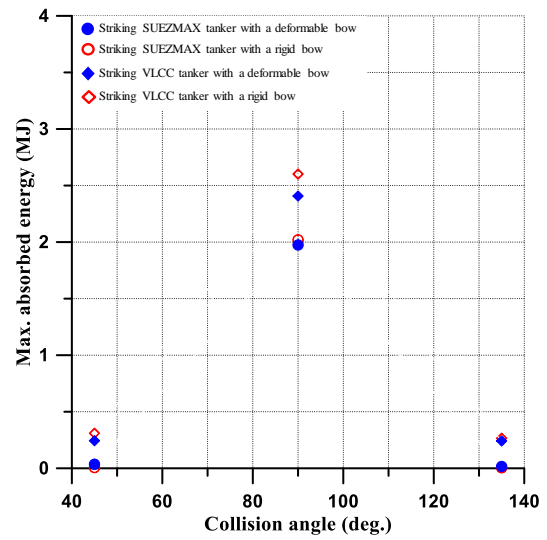


(c)

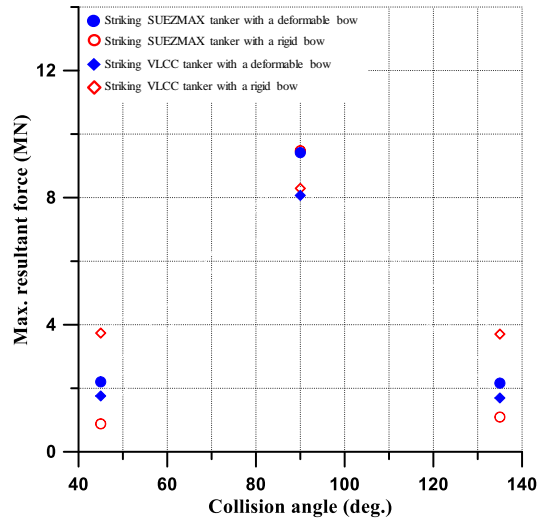
Figure 19(c). The effects of the deformable striking ship bow on the maximum penetration, maximum absorbed energy and maximum resultant force at a collision angle of 135 deg.



(a)

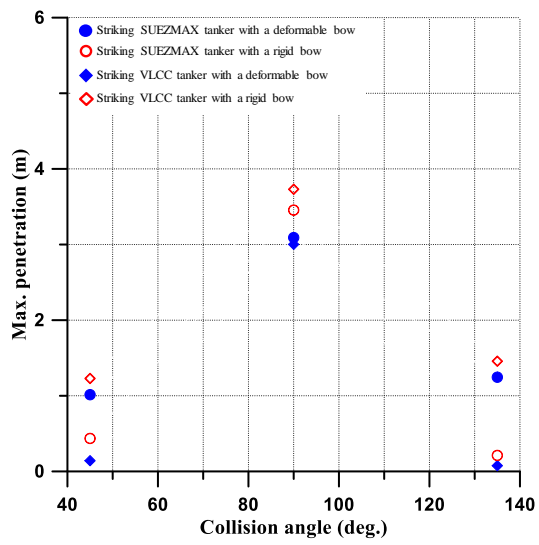


(b)

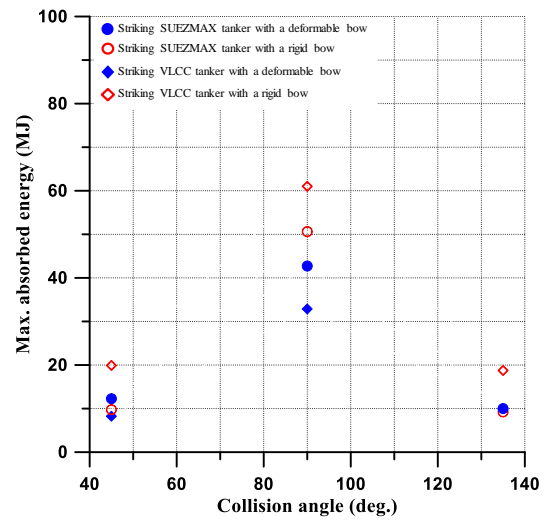


(c)

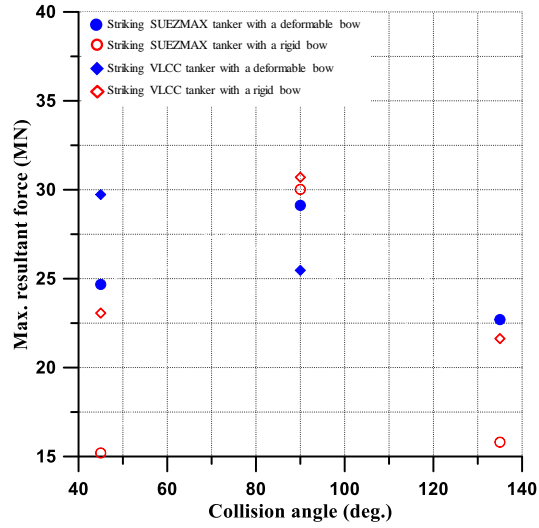
Figure 20(a). The effects of the deformable striking ship bow on the maximum penetration, maximum absorbed energy and maximum resultant force at a collision speed of 0.5 knots.



(a)

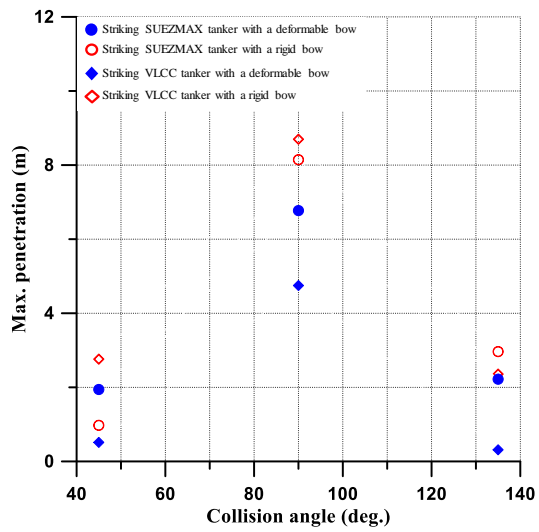


(b)

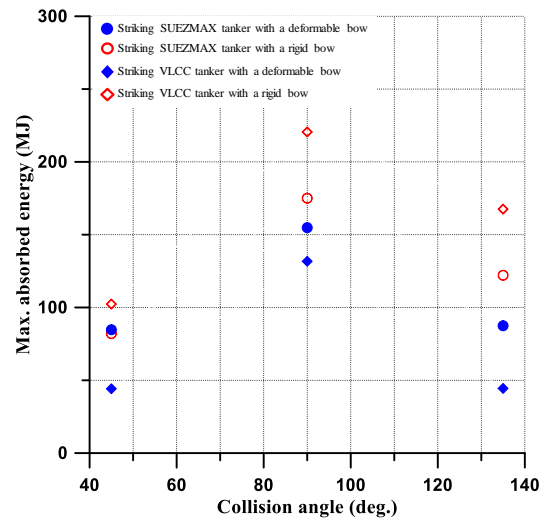


(c)

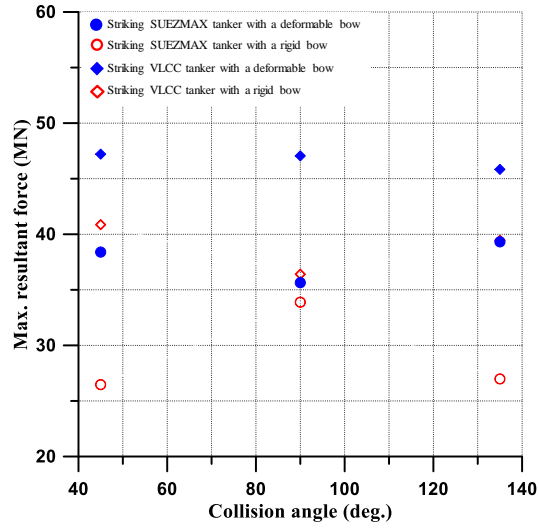
Figure 20(b). The effects of the deformable striking ship bow on the maximum penetration, maximum absorbed energy and maximum resultant force at a collision speed of 3 knots.



(a)

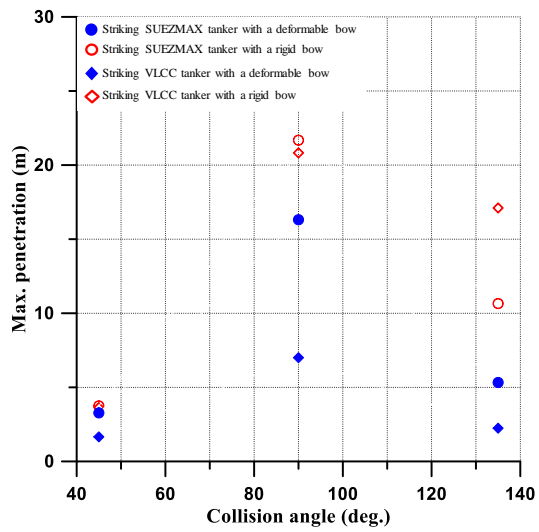


(b)

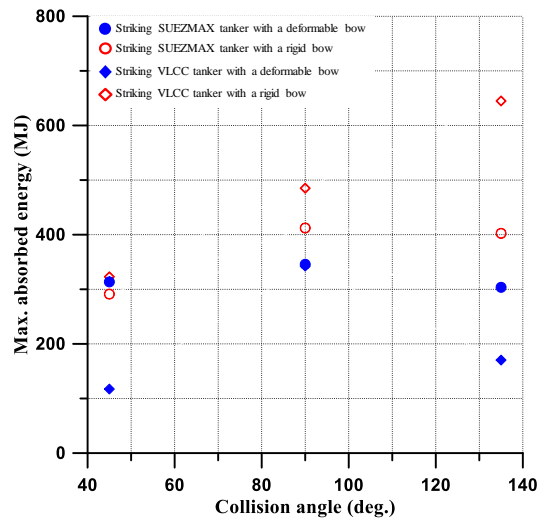


(c)

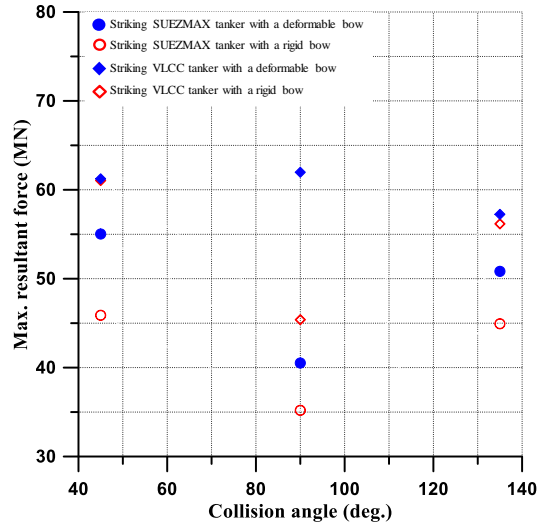
Figure 20(c). The effects of the deformable striking ship bow on the maximum penetration, maximum absorbed energy and maximum resultant force at a collision speed of 6 knots.



(a)



(b)



(c)

Figure 20(d). The effects of the deformable striking ship bow on the maximum penetration, maximum absorbed energy and maximum resultant force at a collision speed of 10 knots.

5. Concluding Remarks

The aim of the present paper has been to examine the effects of a deformable striking ship bow in ship-ship collisions. An extensive study of nonlinear finite element method computations has been undertaken for given collision scenarios in association with the structural crashworthiness where two cases, namely Case A for a collision between a striking VLCC tanker and a struck VLCC tanker and Case B for a collision between a striking SUEZMAX tanker and a struck VLCC tanker, were considered. The angle of collision was varied at 45, 90, and 135 deg. The speed of collision was also varied at 0.5, 3, 6 and 10 knots. The collision location was fixed at the center of the number 3 cargo hold of the struck VLCC tanker. Also, both striking and struck ships were considered to be in a full load condition that can affect the collision location in elevation. A total of 48 scenarios were analyzed by the LS-DYNA nonlinear finite element method. In the industry practice, the striking ship bow is often modeled as a rigid body, but the present study modeled the striking ship bow as a deformable body with the realistic properties of geometry and materials. For a comparison purpose, the rigid body model of the striking ship bow was also considered. Based on the present study, important insights and conclusions can be drawn as follows:

- 1) The rigid bow model of the striking ship results in a greater penetration than the deformable bow model of the striking ship as the striking ship bow structures absorb some part of the initial kinetic energy in the latter model.
- 2) The penetration is the largest at the collision angle of 90 deg. as would be expected.
- 3) The difference of the structural crashworthiness between the deformable and rigid bow models becomes larger as the collision speed increases.
- 4) The shape of the striking ship bow affects the structural damage patterns and the resulting penetration. As the shape of the striking SUEZMAX tanker bow is sharper than that of the striking VLCC tanker bow, the maximum penetration of the former is larger than the latter regardless of the fact that the initial kinetic energy of the latter is greater than that of the former because the displacement of the latter ship is larger than that of the former ship.
- 5) The effects of the deformable striking ship bow are significant in terms of penetration, absorbed energy amount and resultant forces, and should not be neglected in the analysis of structural crashworthiness in ship-ship collisions. Of significance becomes greater as the collision speed becomes faster.

Acknowledgements

The present study was undertaken at the Korea Ship and Offshore Research Institute at Pusan National University which has been a Lloyd's Register Foundation Research Centre of Excellence since 2008.

References

- Alsos HS. 2008. Ship grounding: analysis of ductile fracture, bottom damage and hull girder response [PhD thesis]. Department of Marine Technology, Norwegian University of Science and Technology, Trondheim, Norway.
- Amdahl J. 1983. Energy absorption in ship-platform impacts [PhD thesis]. Department of Marine Technology, Norwegian University of Science and Technology, Trondheim, Norway.
- Ammerman DJ, Daidola JC. 1996. A comparison of methods for evaluating structure during ship collision, Sandia National Labs., Albuquerque, New Mexico, USA
- ANSYS/LS-DYNA. User's manual for ANSYS/LS-DYNA, Version 14.5, ANSYS Inc., New York, USA.
- Bin S, Hu Z, Wang G. 2015. An analytical method for predicting the ship side structure response in raked bow collisions. *Marine Structure*. 41: 288-311.
- Buldgen L, Le Sourne H, Besnard N, Rigo P. 2012. Extension of the super-elements method to the analysis of oblique collision between two ships. *Marine Structure*. 29: 22-57.
- Cowper GR, Symonds PS. 1957. Strain-hardening and strain-rate effects in the impact loading of cantilever beams. Technical Report No. 28, Division of Applied Mathematics, Brown University, Providence, USA.
- Ehlers S, Guird M, Kubiczek J, Hoderath A, Sander F, Sopper R, Charbonnier P, Marhem M, Darie I, von Selle H, Peschmann J, Bendfeldt P. 2016. Experimental and numerical analysis of a membrane cargo containment system for liquefied natural gas. *Ships and Offshore Structures*. 12(S1): S257-S267.
- Ehlers S, Tabri K, Romanoff J, Varsta P. 2010. Numerical and experimental investigation on the collision resistance of the X-core structure. *Ships and Offshore Structures*. 7(1): 21-29.
- Faisal M, Noh SH, Kawsar MRU, Youssef SAM, Seo JK, Ha YC, Paik JK. 2016. Rapid hull collapse strength calculations of double hull oil tankers after collisions. *Ships and Offshore Structures*. 12(5): 624-639.
- Ferry M, Le Sourne H, Besnier F. 2002. MCOL-Theoretical Manual. Technical Report 01-52, French Shipbuilding Research Institute, Nantes.
- Hallquist JO. 2010. LS-DYNA 3D Theory manual, Livermore Software Technology Corporation, CA, USA.
- Haris S, Amdahl J. 2011. An analytical model to assess a ship side during a collision. *Ship and Offshore Structures*. 7(4): 431-448.
- Haris S, Amdahl J. 2013. Analysis of ship-ship collision damage accounting for bow and side deformation interaction. *Marine Structures*. 32: 18-48.
- Hogstrom P, Ringsberg JW. An extensive study of a ship's survivability after collision – A parameter study of material characteristics, non-linear FEA and damage stability analyses. *Marine Structures*. 27: 1-28.
- Hong L. 2008. Simplified analysis and design of ships subjected to collision and grounding, Norwegian University of Science and Technology, Trondheim, Norway.

- Hong L. 2009. Simplified analysis and design of ships subjected to collision and grounding [PhD thesis]. Department of Marine Technology, Norwegian University of Science and Technology, Trondheim, Norway.
- ISSC. 2003. Committee V.3: collision and grounding, Proceedings of 15th International Ship and Offshore Structures Congress, San Diego, USA, 11-15 August 2003.
- ISSC. 2012. Committee V.1: Damage assessment following accidents, International Ship and Offshore Structures Congress (ISSC), Rostock, Germany, 10-13 September 2012.
- Karlsson UB. 2009. Improved collision safety of ships by an intrusion-tolerant inner side shell. *Marine Technology*. 46: 165-173.
- Kim YS, Youssef SAM, Ince ST, Kim SJ, Seo JK, Kim BJ, Ha YC, Paik JK. 2015. Environmental consequences associated with collisions involving double hull oil tanker. *Ship and Offshore Structures*. 10(5): 479–487.
- Kitamura O. 2000. Buffer bow design for the improved safety of ships. Ship Structure Symposium, Virginia, USA.
- Ko YG, Kim SJ, Sohn JM, Paik JK. 2017. A practical method to determine the dynamic fracture strain in nonlinear finite element method computations of ship-ship collisions. Submitted for publication in a journal.
- Kuroiwa T, Kawamoto Y, Kusuba S, Stillman, D. 1995. Numerical Simulation of Collision and Grounding of Ships. Proceedings of MARIENV'95, 66-70.
- Kuroiwa T. 1996. Numerical simulation of actual collision & grounding accidents, Proceedings of International Conference on Design and Methodologies for Collision and Grounding Protection of Ships, San Francisco, USA.
- Le Source H, Couty N, Besnier F, Kammerer C, Legavre H. 2003. LS-DYNA applications in shipbuilding, Proceedings of 4th European LS-DYNA Users Conference. 1-16.
- Liu B, Villavicencio R, Soares CG. 2013. Experimental and numerical plastic response and failure of laterally impacted rectangular plates. *Journal of Offshore Mechanics and Arctic Engineering*. 135: 1-7.
- Montewka J, Goerlandt F, Ehlers S, Kunjala P, Erceg S, Polic D, Klanac A, Hinz T, Tabri K. 2012. Sustainable Maritime Transportation and Exploitation of Sea Resources. Taylor & Francis, London, UK.
- Ozguç O, Das PK, Barltrop N. 2005. A comparative study on the structural integrity of single and double side skin bulk carriers under collision damage. *Marine Structures*. 18: 511-547.
- Parunov J, Rudan S, Corak M. 2016. Ultimate hull-girder-strength-based reliability of a double-hull oil tanker after collision in the Adriatic Sea. *Ship and Offshore Structures*. 12(S1): S55-S67.
- Paik JK. 2007a. Practical techniques for finite element modeling to simulate structural crashworthiness in ship collisions and grounding (Part I: Theory). *Ships and Offshore Structures*. 2(1): 69-80.
- Paik JK. 2007b. Practical techniques for finite element modeling to simulate structural crashworthiness in ship collisions and grounding (Part II: Verification). *Ships and Offshore Structures*. 2(1): 81-86.
- Paik JK, Thayamballi AK. 2003. Ultimate limit state design of steel plated structures. Wiley, Chichester.
- Paik JK, Thayamballi AK. 2007. Ship-shaped offshore installation: design, building and operation, Cambridge University Press, Cambridge, London.
- Paik JK, Park JH, Samuelides E. 2009. Collision accidental limit states performance of double hull oil tanker structures: Pre-CSR versus CSR designs. *Marine Technology*. 46: 183-191.

- Pedersen PT. 1993. Ship impacts: Bow collision. *International Journal of Impact Engineering*. 13: 163-187.
- Pedersen PT, Zhang S. 1998. On Impact Mechanics in Ship Collisions. *Journal of Marine Structures*. 11(10): 429-449.
- Sajdak J, Brown A. 2004. Modeling longitudinal damage in ship collisions, Technical Report No. SSC-437, Ship Structural Committee, Washington D.C, USA.
- Simonsen BC. 1997. Mechanics of ship grounding [PhD thesis]. Department of Naval Architecture and Offshore Engineering, Technical University of Denmark, Lyngby, Denmark.
- Storheim M, Amdahl J. 2014. Design of offshore structures against accidental ship collisions. *Marine Structures*. 37: 135-172.
- Storheim M, Amdahl J. 2015. On the sensitivity to work hardening and strain-rate effects in nonlinear FEM analysis of ship collisions. *Ship and Offshore Structures*. 12(1): 100-115.
- Storheim M, Alsos HS, Hopperstad OS, Amdahl J. 2015. A damage-based failure model for coarsely meshed shell structures. *International Journal of Impact Engineering*. 83: 59–75.
- Tavakoli MT, Amdahl J, Leira BJ. 2010. Analytical and numerical modelling of oil spill from a side tank with collision damage. *Ship and Offshore Structures*. 7(1): 73-86.
- Tornqvist R. 2003. Design of crashworthy ship structures [PhD thesis]. Department of Naval Architecture and Offshore Engineering. Technical University of Denmark, Lyngby, Denmark.
- Urban J. 2003. Crushing and fracture of lightweight structures [PhD thesis]. Department of Mechanical Engineering, Technical University of Denmark, Lyngby, Denmark.
- Villavicencio R, Kim YH, Cho SR, Guedes Soares C. 2013. Deformation process of web girders in small-scale tanker double hull structures subjected to lateral impact. *Marine structures*. 32: 84-112.
- Wisniewski K, Kolakowski P. 2002. The effect of selected parameters on ship collision results by dynamic FE simulations. *Finite Elements in Analysis and Design*. 39: 985-1006.
- Yamada Y, Endo H. 2008. Experimental and numerical study on the collapse strength of the bulbous bow structure in oblique collision. *Marine Technology*. 45:42–53.
- Youssef SAM, Faisal M, Seo JK, Kim BJ, Ha YC, Kim DK, Paik JK, Cheng F, Kim MS. 2014. Assessing the risk of ship hull collapse due to collision. *Ship and Offshore Structures*. 11(4): 335-350.
- Youssef SAM, Noh SH, Paik JK. 2017. A new method for assessing the safety of ships damaged by collisions. *Ship and Offshore Structures*. (<http://dx.doi.org/10.1080/17445302.2017.1285679>)
- Zhang S. 1999. The mechanics of ship collisions [PhD thesis]. Department of Naval Architecture and Offshore Engineering, Technical University of Denmark, Lyngby, Denmark.
- Zhang S, Villavicencio R, Zhu L, Pedersen PT. 2016. Impact mechanics of ship collisions and validations with experimental results. *Marine structures*. 52: 69–81.
- Zheng Y, Aksu D, Vassalos, Tuzcu C. 2007. Study on side structure resistance to ship-ship collision. *Ship and Offshore Structures*. 2(3): 273–293.